國 立 交 通 大 學
電信工程研究所
碩士論文

應用於系統封裝之立體平面倒 F 天線設計

Design of On-Package Planar Inverted-F Antenna
for RF System-on-Package Application

研究生：李嘉祐

指導教授：鍾世忠博士

中華民國九十四年六月

Design of On-Package Planar Inverted-F Antenna for RF System-on-Package Application

研究生：李嘉祐　　Student：Chia-Yu Lee

指導教授：鍾世忠 博士　　Advisor：Dr. Shyh-Jong Chung

國立交通大學

電信工程研究所

碩士論文

A Thesis

Submitted to Institute of Communication

College of Electrical Engineering and Computer Science

National Chiao Tung University

In Partial Fulfillment of the Requirements

for the Degree of Master of Science

In

Communication Engineering

June 2005

中華民國九十四年六月

應用於系統封裝之立體平面倒 F 天線設計

研究生：李嘉祐　　指導教授：鍾世忠博士

國立交通大學 電信工程學系研究所

碩士論文

摘要

本篇論文提出一個應用於系統封裝的平面倒 F 天線，這是一個和屏閉金屬盒整合在一起的立體天線，並且是由單一的金屬片摺疊，一體成型。這個天線具有6.55%的頻寬，從 2.37GHz 到 2.53 GHz，在 x-z 平面具有全向性的輻射場型，平均輻射增益是-0.63dBi。天線的尺寸是 $20 \times 15 \times 3.5$ mm^3，接地面積是 20×40 mm^2。此外，由於屏閉金屬盒也是天線的一部分，我們討論在屏閉金屬盒內部的電路和天線之間耦合的關係。我們發現在金屬盒內部的電路和天線彼此之間不會太會影響，並且可以經由適當擺放電路在金屬屏閉盒裡的位置，達到非常良好的隔離度。在距離天線饋入點愈遠的地方，隔離度愈好。

Design of On-Package Planar Inverted-F Antenna for RF System-on-Package Application

Student：Chia-Yu Lee Advisor：Dr. Shyh-Jong Chung

Institute of Communication Engineering

National Chiao Tung University

ABSTRACT

In this thesis, an on-package planar inverted-F antenna for RF system-on-package (SOP) application was proposed. The on-package planar inverted-F antenna (PIFA) consists of a single folded copper plate. The proposed antenna has achieved the impedance bandwidth of 6.55% from 2.37 to 2.53 GHz and an average gain of -0.63dBi at x-z plane. The dimension of this antenna is 20 × 15× 3.5 mm^3, and the ground size is 20 × 40 mm^2. In addition, we investigate the coupling effect between the on-package PIFA and the RF components in the shielding package. It was observed that the antenna performance has merely change and the best isolation between the antenna and RF components can be achieved when the components have been appropriately arranged in the package.

Acknowledgement

首先感謝老師，能夠依照個人的興趣給予發展，同時對於個人的想法有極大的包容。另外，老師待人敦厚、親切，這也一直是我學習的典範。我想，我個人最大的收穫就是老師對各方面都能充滿活力並且努力面對，相信對我未來相當的有幫助。

同時也要感謝謝昀錚學長、凌菁偉學姊、饒珮宗學長，王侑信、邱珮如、吳民仲和陳清文同學，徐民峰、林克強、張均富、洪崇喻、陳煥能等學弟，還有助理陳珮華，大家在實驗室中互相學習、討論。

最後感謝我的父母和家人，給我不斷的支持和鼓勵，讓我無後顧之憂，盡情學習。

Content

Table List

Figure List

Chapter 1

Introduction

1.1 Motivation

Wireless transceivers are required to support multiple frequency band, wider bandwidth and multi-standard for future communications. Also the RF module has to provide high efficiency, low noise, and small size. System-on-Package (SOP) technology is one of the solutions for future wireless transceiver module. SOP can give flexibility to the transceiver module by integrating all functional blocks with the multi-layer process and the novel interconnection methods [1].

Basic wireless transceiver components are composed of an antenna, a radio, and a baseband processor. The radio was largely discrete and now is usually implemented as multichip module with gallium arsenide (GaAs) for the power amplifier (PA) and perhaps for the low-noise amplifier (LNA) and bipolar or BICMOS for the mixer and intermediate frequency functions. The baseband processor was realized with general-purpose complementary metal-oxide-semiconductor (CMOS) integrated circuits and now is always implemented with special-purpose CMOS integrated circuits. For the dominance of CMOS in the electronics industry and the steady improvement in the radio frequency performance of CMOS, people have much interest in the integration of the radio with the baseband processor into a single CMOS chip. There have been many single-chip wireless transceivers, such as those fabricated in 0.25-μm at 1.8 GHz for DCS-1800 applications and at 2.45 GHz for Bluetooth applications [2], [3]. Single-chip solutions for the wireless transceivers have employed the zero- or IF architectures. Therefore, the difficulty of the integration of different high-Q analogy band pass filters for band selection and for

channel selection has been avoided. But, not all integration problems can be overcome or avoided by the proper architectures. For example, there are the antenna filter for spurious emission suppression and the antenna itself for efficient radiation. They are independent of the wireless transceiver architectures and currently couldn't be combined into a single silicon chip within several square millimeters. Consequently, they are left external to the single silicon chip in all solutions of highly integrated wireless systems.

One of the major issues for developing SOP is efficiently integrating an antenna with a module. Fabricating an antenna directly on the package has the advantage of reducing feeder loss and size of the entire module. Wireless modules including an antenna in the package have been developed for mimimeter-wave frequency band. Nevertheless, for lower frequency band such as C-band, it is difficult to put an antenna into the module since the size of the antenna becomes large. Moreover there are issues to be solved such as narrow bandwidth in ceramic packaging and interference between the antenna and the other RF blocks in highly integrated module [1], [4].

In this thesis, an on-package planar inverted-F antenna for RF SOP application was proposed. The on-package PIFA consists of a single folded copper plate. The proposed antenna has achieved the impedance bandwidth of 6.55% from 2.37 to 2.53 GHz and an average gain of -0.63dBi at x-z plane. The dimension of this antenna is $20 \times 15 \times 3.5\ mm^3$, and the ground size is $20 \times 40\ mm^2$. In addition, we investigate the coupling effect between the on-package PIFA and the RF components in the shielding package. It was observed that the antenna performance has merely change and the best isolation between the antenna and RF components can be achieved when the components have been appropriately arranged in the package.

1.2 Organization

This thesis is devoted to the on-package planar inverted-F antenna for RF SOP application. It consists of five chapters. Chapter 1 gives the introduction of SOP approach and the motivation of this thesis. In Chapter 2, we introduce basic theory of patch antennas and planar inverted-F antennas. Chapter 3 exhibits the design methodology and measurement of the on-package PIFA. In Chapter 4, the coupling effects between the on-package PIFA and RF components are investigated. Chapter 5 shows the conclusions of the excellent antenna in this thesis. The references are attached in the end.

Chapter 2

Theory of Patch Antennas and Planar Inverted-F Antennas

2.1 Patch Antennas

A microstrip device is a layered structure with two parallel conductors separated by a thin dielectric substrate and the lower conductor acting as a ground plane. If the upper metallization is a patch that is an appreciable fraction of a wavelength in extent, the devices becomes a microstrip antenna, as illustrated in Fig 2-1. The patch antenna belongs to the class of resonant antennas and its resonant behavior is responsible for the main challenge in microstrip antenna design-achieving adequate bandwidth.

The fringing fields act to extend the effective length of the patch and are responsible for the radiation. The fringing field and the radiation loss at the open-end of the microstrip line can be represented by the equivalent capacitive component B_0 and conductive component G_0, respectively, as shown in Fig 2-2.

$$G_0 = \begin{cases} \dfrac{W}{90\lambda^2}, & W < 0.35\lambda \\ \dfrac{W}{120\lambda} - \dfrac{1}{60\pi^2}, & 0.35\lambda \le W \le 2\lambda \\ \dfrac{W}{120\lambda}, & W > 2\lambda \end{cases} \tag{2-1}$$

$$B_0 = \frac{\tan \beta \Delta l}{Z_0} \approx \beta \frac{\Delta l}{Z_0} \tag{2-2}$$

The patch antenna is usually operated near resonance in order to obtain a real-valued input impedance. Fig 2-3 shows the transmission-line model of the microstrip patch antenna. This model can be used to determine the resonant frequency or the total length of the patch. The input admittance of the fed of the patch antenna is given by

$$Y_{in} = Y_0 \frac{(G_0 + B_0) + jY_0 \tan \beta L_1}{Y_0 + j(G_0 + B_0)\tan \beta L_1} + Y_0 \frac{(G_0 + B_0) + jY_0 \tan \beta L_2}{Y_0 + j(G_0 + B_0)\tan \beta L_2} \tag{2-3}$$

When the total length L of a microstrip patch antenna is

$$L = L_1 + L_2 \approx \frac{\lambda_d}{2} = \frac{\lambda}{2\sqrt{\varepsilon_r}} \tag{2-4}$$

, the patch antenna is resonant, where λ is the free-space wavelength, λ_d the wavelength in the dielectric and ε_r the substrate dielectric constant. The expression for the input impedance (reactance is zero at resonance) of the resonant patch is

$$Z_{in} = \frac{R_0}{2}\cos^2(\beta L_1) \qquad ; R_0 = \frac{1}{G_0} \tag{2-5}$$

The patch length L for resonance is given by approximately half wavelength and the patch width W is selected to given the proper radiation resistance at the input, often 50Ω. The far-field components are

$$\begin{aligned} E_\theta &= E_0 \cos\phi \, f(\theta, \phi) \\ E_\phi &= -E_0 \cos\theta \, \sin\phi \, f(\theta, \phi) \end{aligned} \tag{2-6}$$

where

$$f(\theta, \phi) = \frac{\sin\left[\frac{\beta W}{2}\sin\theta \, \sin\phi\right]}{\frac{\beta W}{2}\sin\theta \, \sin\phi} \cos\left[\frac{\beta L}{2}\sin\theta \, \cos\phi\right] \tag{2-7}$$

The principal plane patterns follow the above equation as

$$\begin{aligned} F_E(\theta) &= \cos\left(\frac{\beta L}{2}\sin\theta\right) && \text{E-plane, } \phi = 0^0 \\ F_H(\theta) &= \cos\theta \frac{\sin\left[\frac{\beta W}{2}\sin\theta\right]}{\frac{\beta W}{2}\sin\theta} && \text{H-plane, } \phi = 90^0 \end{aligned} \tag{2-8}$$

The length of the half-wave patch antenna can be halved by placing a short-circuit plate between the patch and ground plane at the center of the patch where the fields are zero. The modified antenna is called as a planar inverted-F antenna [5], [6].

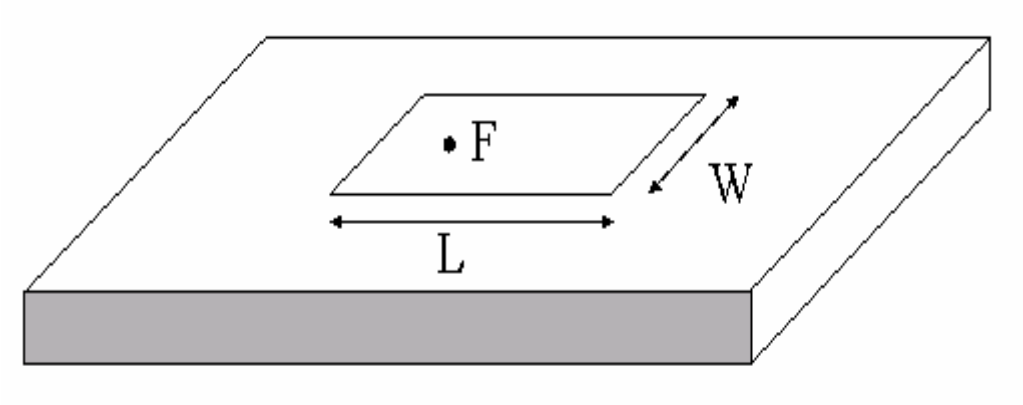

Fig 2-1 Geometry for the microstrip patch antenna.

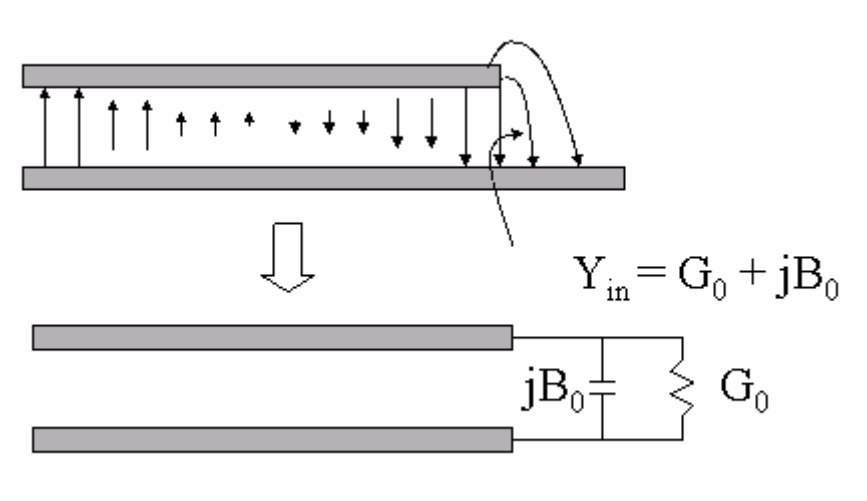

Fig 2-2 Equivalent components for the fringing field and the radiation loss.

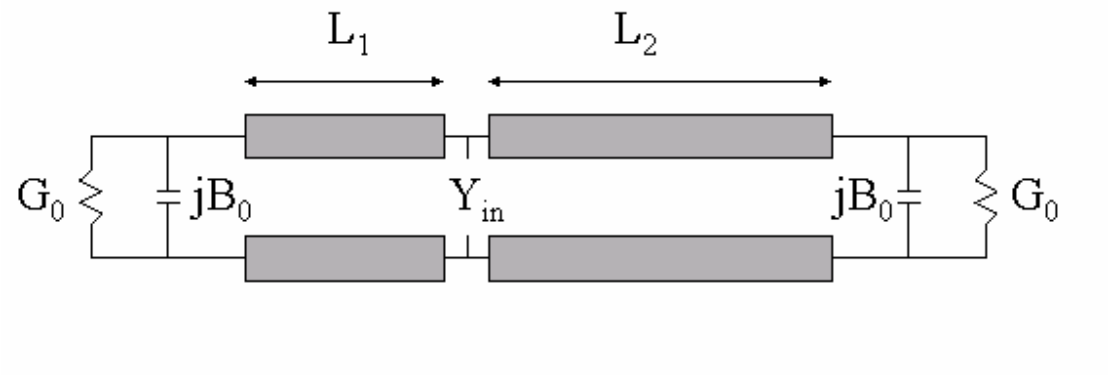

Fig 2-3 Transmission-line model of the microstrip patch antenna.

2.2 Planar Inverted-F Antennas

There have been frequent requests to develop small antennas for the further miniaturization of portable mobile phone sets. Thus, antennas having small and low profile structures are suitable for mounting on portable equipment. Among these antennas, the planar inverted-F antenna (PIFA) is one of the most promising. The PIFA typically consists of a rectangular planar element, ground plane, and short-circuit plate of narrower width than that of a shortened side of a planar element. Fig 2-4 shows the structure of the PIFA. The PIFA can be considered as a kind of short-circuit rectangular microstrip antenna (or liner inverted-F antenna with the wire radiator element replaced by a plate to expand the bandwidth).

Fig 2-5 shows the transmission-line model of the planar inverted-F antenna. The resonant frequency (or the total length of the radiating element) can be determined by this model. The input admittance of the fed of the PIFA is

$$Y_{in} = -jY_0 \cot \beta L_1 + Y_0 \frac{(G_0 + B_0) + jY_0 \tan \beta L_2}{Y_0 + j(G_0 + B_0)\tan \beta L_2} \tag{2-9}$$

When the total length L of the radiating element is

$$L = L_1 + L_2 \approx \frac{\lambda_d}{4} = \frac{\lambda}{4\sqrt{\varepsilon_r}} \tag{2-10}$$

, the PIFA is resonant, where ε_r is the substrate dielectric constant, λ_d the wavelength in the dielectric and λ is the free-space wavelength. The input impedance of the resonant PIFA is given by

$$Z_{in} = R_0 \cos^2(\beta L_2) \qquad ; R_0 = \frac{1}{G_0} \tag{2-11}$$

The radiation resistance of the PIFA is twice that of the half-wave patch antenna. The resonant frequency determined by the model is exact in case of $W_s/W = 1$.

As shown in Fig 2-6, the current on the undersurface of the planar element mainly flows to the open-circuit edge on the long side of the planar element in the case of

$W\text{-}W_s < L$. However, the current flows to the open-circuit edge on the short side of the planar element in the case of $W\text{-}W_s > L$. According to the analysis results for the surface current, one can assume that the effective length of the current flow on the short-circuit plate and planar element. Then, in the case of $W_s/W = 1$, the resonance is expressed by

$$L + H = \frac{\lambda}{4} \tag{2-12}$$

and in case of $W_s = 0$, it is expressed by

$$L + W + H = \frac{\lambda}{4} \tag{2-13}$$

In case of $0 < W_s/W < 1$, the resonant frequency f_r can be expressed by

$$f_r = r \cdot f_1 + (1 - r) \cdot f_1 \quad \text{for} \quad \frac{W}{L} \leq 1 \tag{2-14a}$$

and

$$f_r = r^k \cdot f_1 + (1 - r^k) \cdot f_1 \quad \text{for} \quad \frac{W}{L} \geq 1 \tag{2-14b}$$

where $r = W_s/W$, $k = W/L$, and resonance for frequency f_1 is expressed by (2-12). Resonance for frequency f_2 is expressed by (2-13) [6], [7].

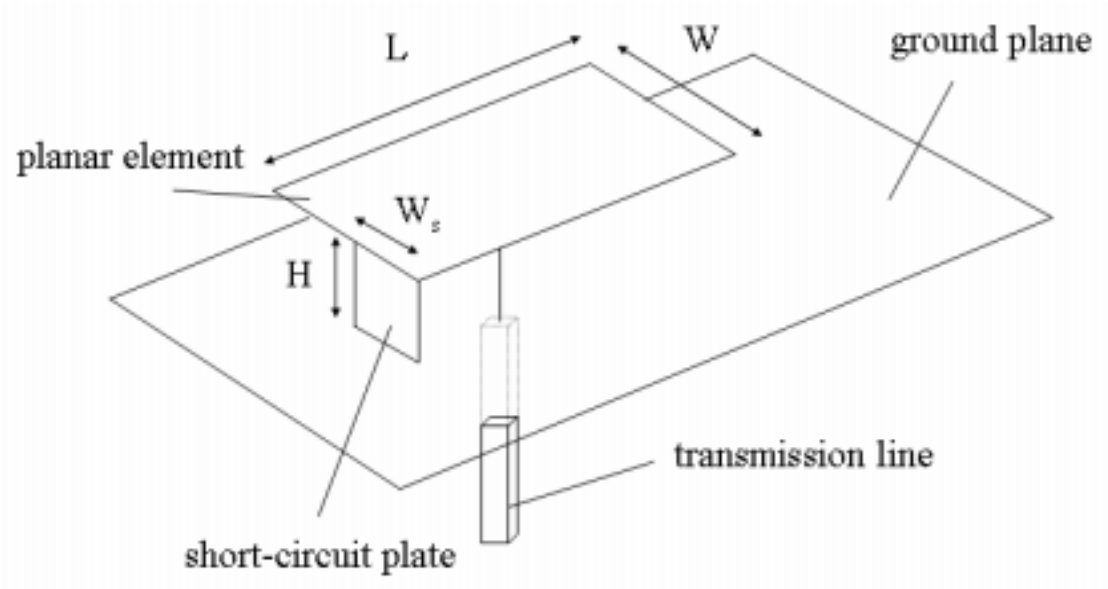

Fig 2-4 Structure for the planar inverted-F antenna.

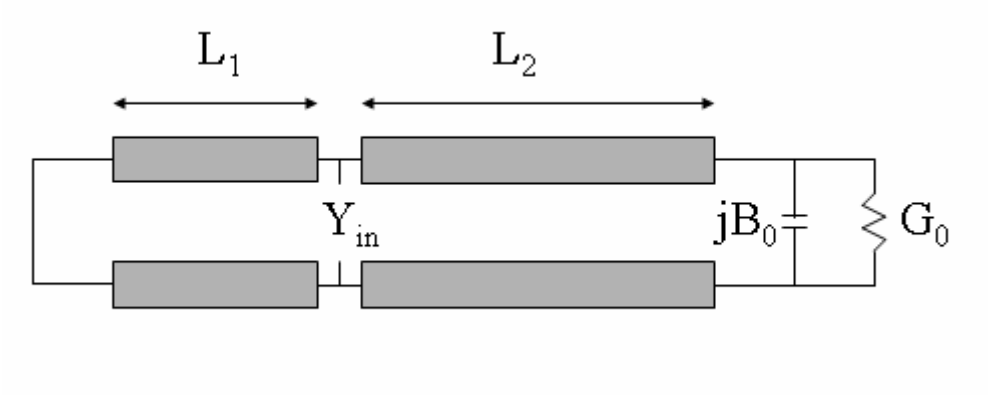

Fig 2-5 Transmission-line model of the planar inverted-F antenna.

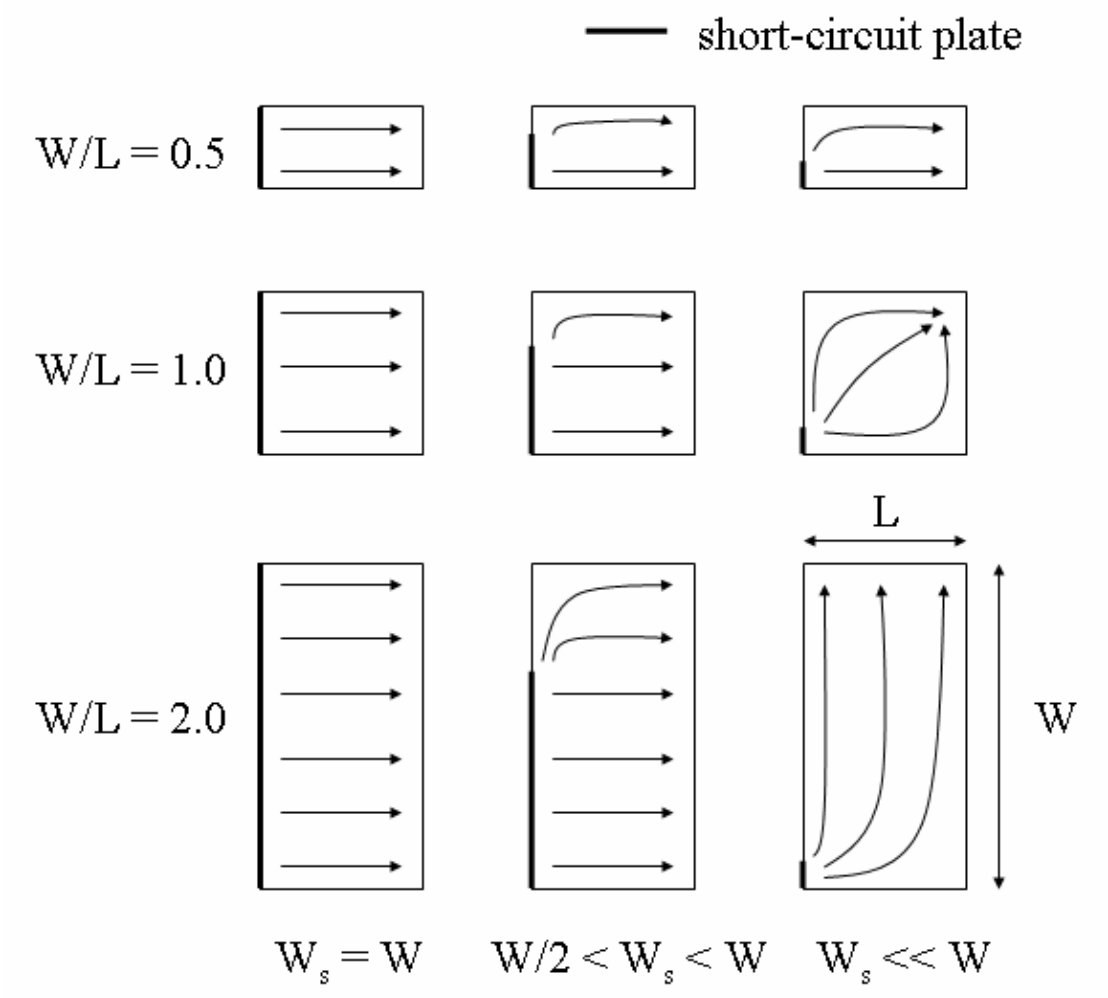

Fig 2-6 Variation of surface current flow on planar element due to size ratio of planar element and width of short-circuit plate.

Chapter 3

Design and Measurement of On-Package PIFA

3.1 Design of On-Package PIFA with and without Dielectric Material

In general, antennas for portable wireless transceivers are based around either a retractable whip monopole or an encapsulated helix because of their simple structures and high radiation gains. However, neither the monopole nor the helical antenna can be neatly integrated with the rest of a wireless transceiver. Recently many patch antennas integrated with package are implemented with the low temperature co-fired ceramic (LTCC) package or the ceramic ball grid array package (CBGA) [8]-[12]. But a patch antenna can not be integrated with package using a single folded copper plate. Consequently, the preferred candidate is the planar inverted-F antenna.

In this thesis, we utilize the planar inverted-F antenna to achieve the desired antenna integrated with package using a single folded copper plate. As for the rapidly growing wireless market, the demand for compact and low-cost antennas becomes more and more urgent. This designed antenna is applied for IEEE 802.11b/g WLAN. The required bandwidth should cover the band from 2.4~2.4835 GHz when input return loss is below -10dB. The on-package planar inverted-F antenna is implemented on the FR4 substrate, whose dielectric constant is 4.7, loss tangent is 0.02, and thickness is 0.8 mm. The specifications of the on-package PIFA are listed bellow:

The height of PIFA is less than 3mm.

The package is $15 \times 15 \times 1.5\ mm^3$.

The ground size is $20 \times 40\ mm^2$.

The feed of PIFA must be located at the edge of the package..

3.1.1 On-Package PIFA with Dielectric Material

Single-chip wireless transceivers in their bare forms are susceptible to the effect of mechanical stress, environmental change, and electrostatic discharge. Therefore, they are packaged with dielectric materials. We will introduce an on-package planar inverted-F antenna with a ceramic material. The on-package PIFA can be integrated with a wireless transceiver bare chip to achieve a WLAN module. Furthermore, the RF circuits including an antenna are integrated as a single packaged chip.

The on-package PIFA can be realized by a single folded copper plate. The antenna has several advantages of light weight, low-cost and easy fabrication. The feed of the on-package PIFA must be located at the edge of the package. The restriction of the fabrication technology must be taken into consideration. For example, the short-circuit plate and the feed line can not be arranged too close to each other. If the gap is too small, it can not be realized with the technology. The structure of the planar inverted-F antenna is indicated in Fig 3-1 and the lateral views are shown in Fig 3-2.

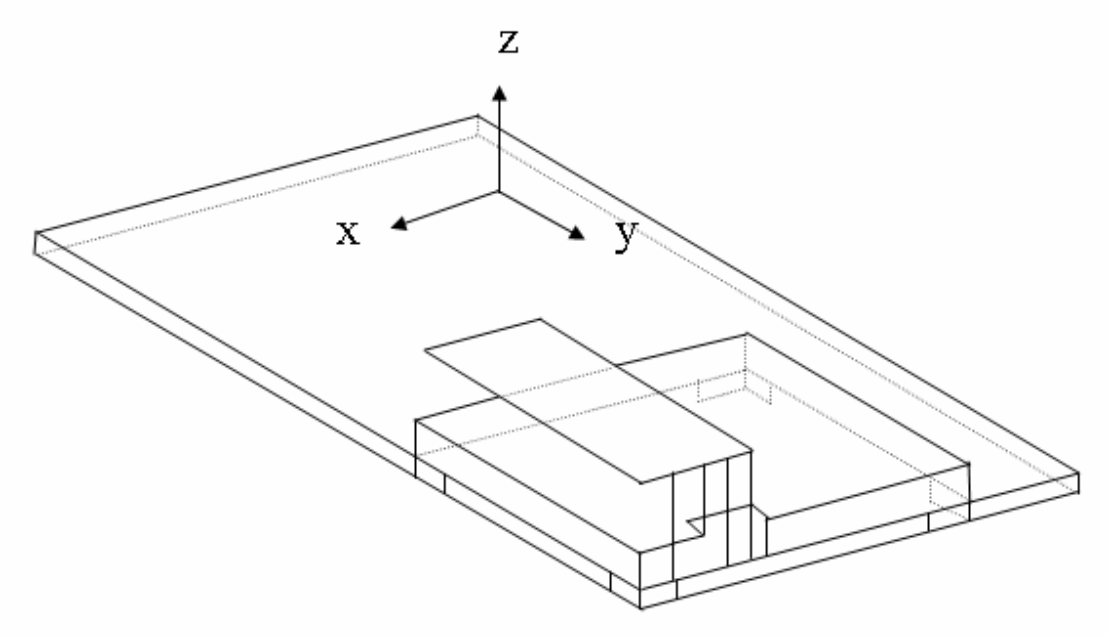

Fig 3-1 3-D structure of the on-package PIFA with dielectric material.

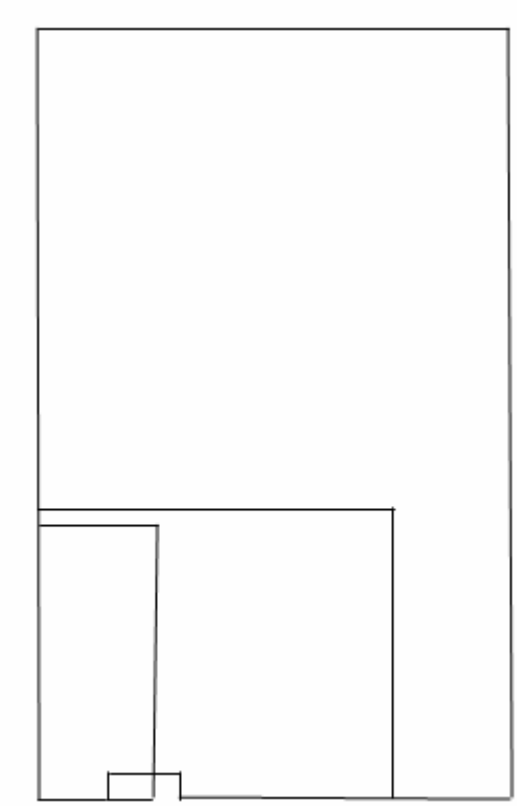

Fig 3-2a

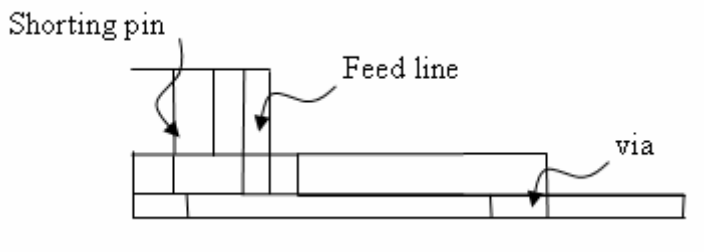

Fig 3-2b

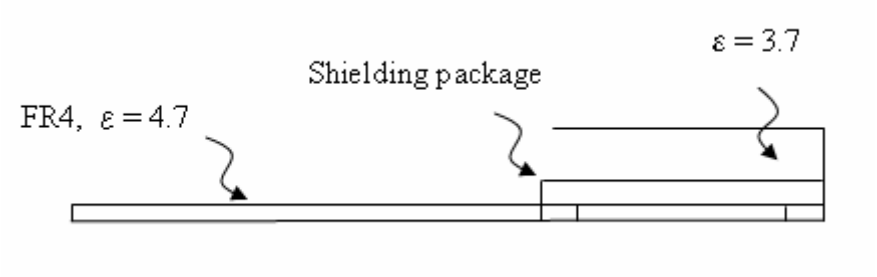

Fig 3-2c

Fig 3-2 Lateral views of the on-package PIFA with dielectric material (a) x-y plane (b) x-z plane (c) y-z plane.

The length l and width w of the on-package PIFA determine the resonant frequency, which can be approximated by the formula

$$f_0 = \frac{v}{4(w+l)}$$

where

v is the wave velocity in the ceramic material;

l and w are the length and width of the radiating element;

f_0 is the resonant frequency.

The radiating element is grounded by a short-circuit strip and fed near the short-circuit strip with the feed line. The input impedance of the antenna can be easily matched to 50Ω by controlling the feed position relative to the short-circuit strip.

In the packaging process, the shielding package and the antenna are filled with a dielectric material whose dielectric constant is 3.7 and loss tangent is 0.018. The other characteristics of PCB and specifications of the shielding package are mentioned above. The dielectric material is extremely critical to the performance of the bandwidth and the gain for the antenna. The patch size of the antenna is 5×14.3 mm^2 and the height is 3 mm. The short-circuited strip is located on the edge of the patch and 1.5mm apart from the corner. The width of the short pine is 1.5mm and the height is 3mm. The width of the feed line is 1 mm and the height is 4.5mm. The gap between the short pine and the feed line is 1mm.

The configuration of the on-package PIFA is a three-dimensional structure. Thus, we can apply the 3-D full-wave EM simulator Ansoft HFSS 8.0 to simulate the on-package PIFA. The simulated input return loss and the radiation pattern are shown in Fig 3-3 and Fig 3-4, respectively. It has 120MHz bandwidth from 2.39 to 2.51 GHz when the input return loss is bellow -10dB. The bandwidth can cover IEEE 802.11b/g WLAN band from 2.40 to 2.4835 GHz. At x-z plane, the radiation pattern

is omnidirectional. The maximum gain and average gain are 3.52dBi and 1.50dBi, respectively. The gains of each plane at 2.45GHz are listed in Table 3-1.

	x-z plane	y-z plane	x-y plane
Maximum Gain	3.52dBi	3.52dBi	2.54dBi
Average Gain	1.50dBi	-2.31dBi	-2.32dBi

Table 3-1 The maximum and average gain of the on-package PIFA with dielectric material at 2.45GHz.

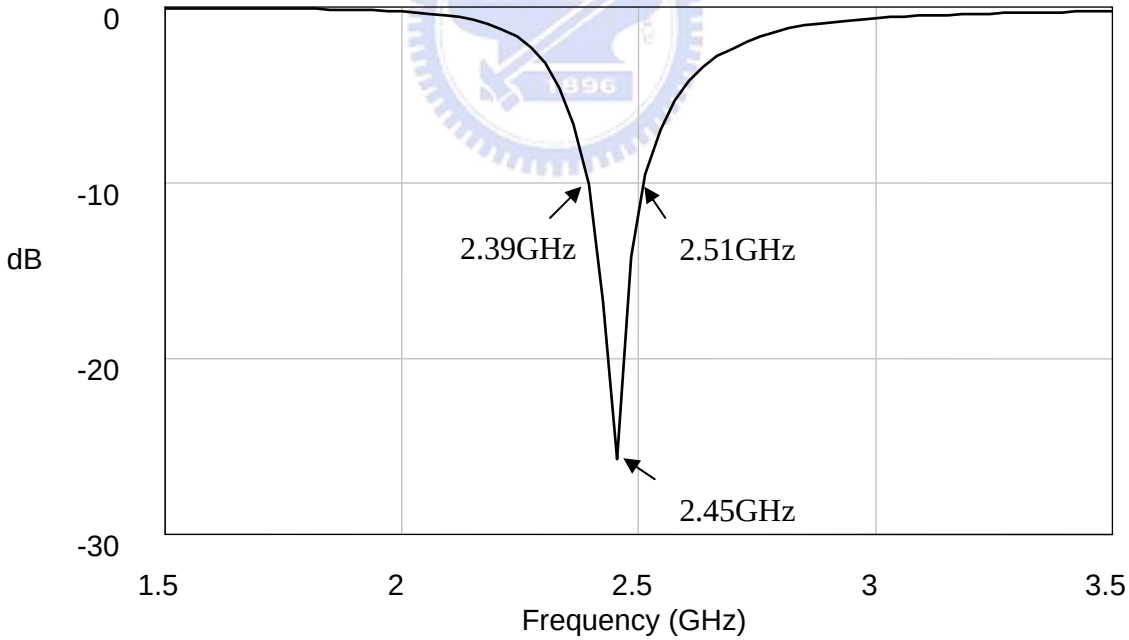

Fig 3-3 Return loss of the on-package PIFA with dielectric material.

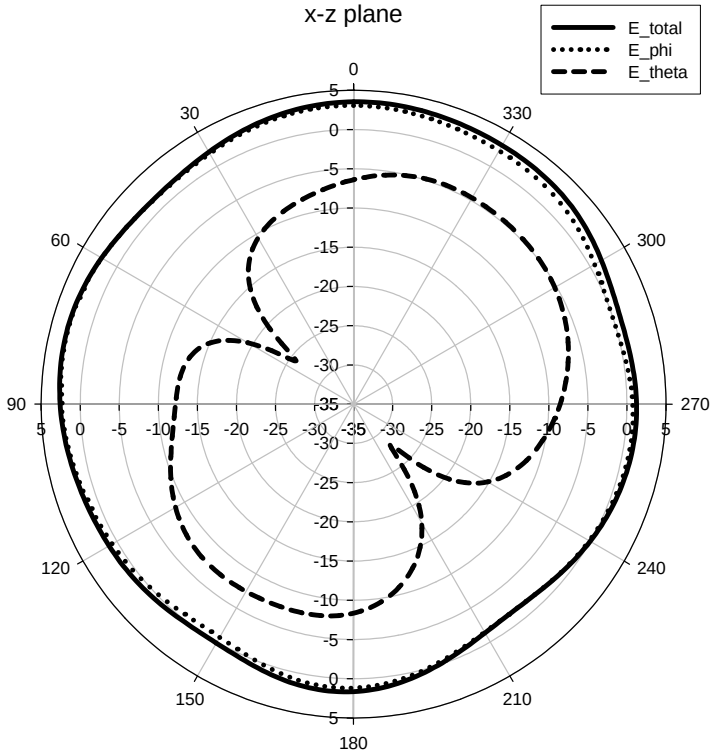

Fig 3-4a Radiation pattern of on-package PIFA with dielectric material at x-z plane (2.45GHz).

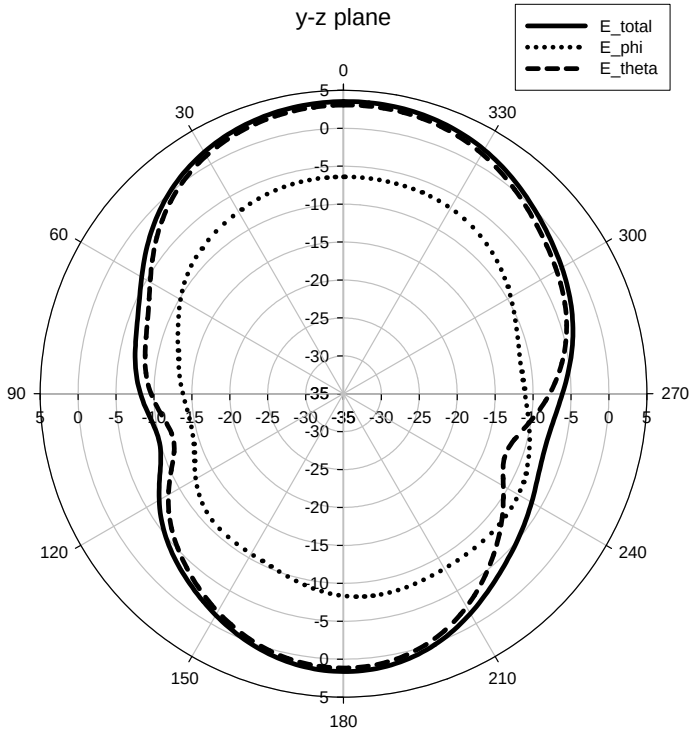

Fig 3-4b Radiation pattern of on-package PIFA with dielectric material at y-z plane (2.45GHz).

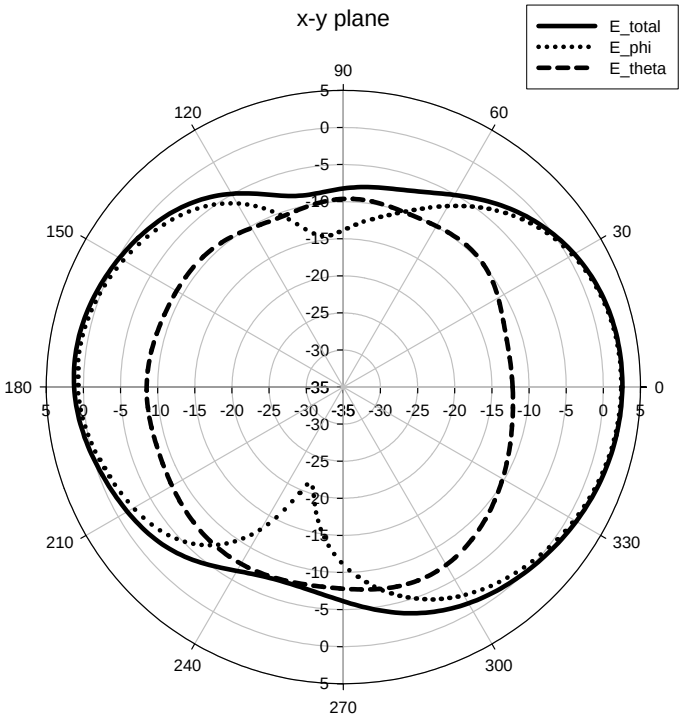

Fig 3-4c Radiation pattern of on-package PIFA with dielectric material l at x-y plane (2.45GHz).

3.1.2 On-Package PIFA in Air

As described in section 3.1, the on-package PIFA with dielectric material has the advantage of being integrated with a wireless transceiver bare chip. Besides, we can use the discrete components to complete the RF circuit and the packaging dielectric material can be excluded. The bandwidth and the gain of the antenna can also be increased without the dielectric material. In this section, we removed the filled dielectric material in the shielding package and leave the PIFA in air. Another advantage of dropping the dielectric material is that if the bandwidth has been enough wider than the IEEE 802.11b/g WLAN band, we could reduce the height of the antenna to minimize the package totally size. In addition, the space next to the shielding package is not efficiently used. We extend it to the edge of the FR4 board to form a new shielding package with the size of $15 \times 20 \times 1.5\ mm^3$. We have improved the on-package PIFA in Section 3.1 and the new antenna can be still embedded into the shielding package. The structure of the new on-package PIFA is indicated in Fig 3-5 and the lateral views are shown in Fig 3-6.

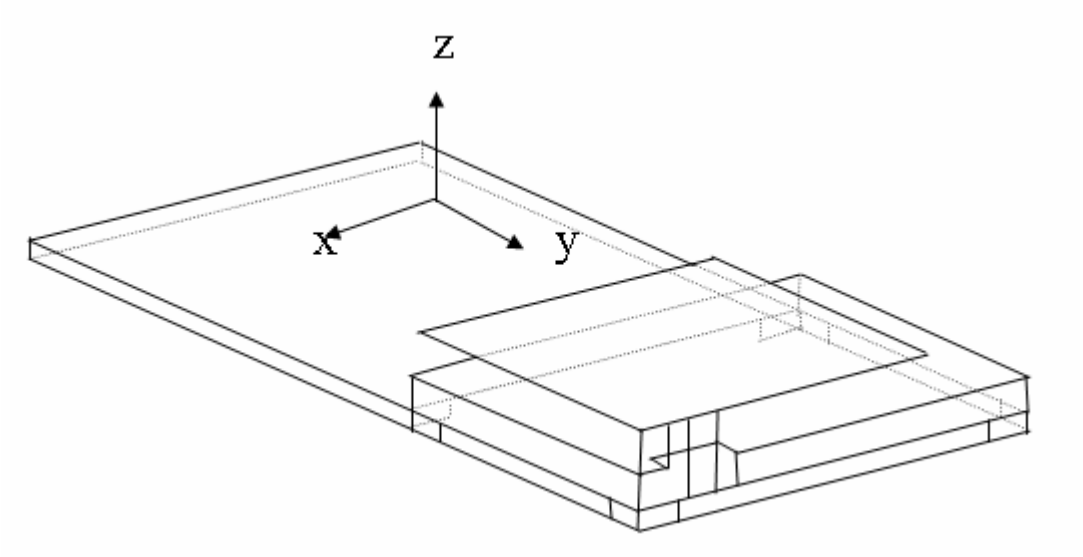

Fig 3-5 3-D structure of the on-package PIFA in air.

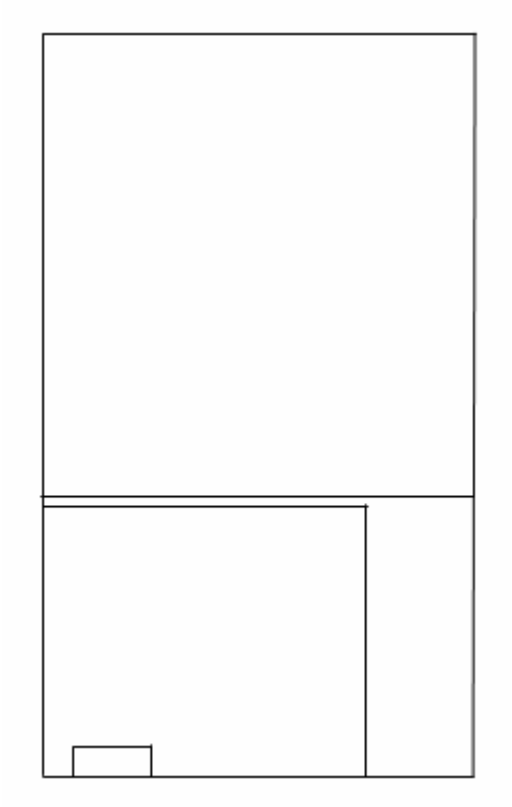

Fig 3-6a

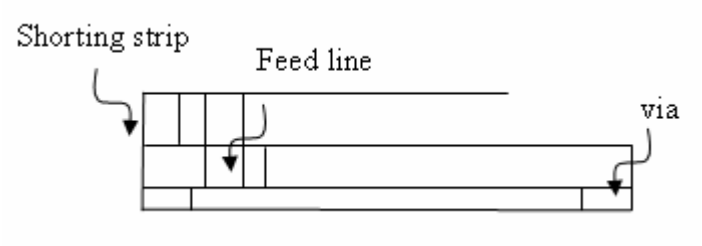

Fig 3-6b

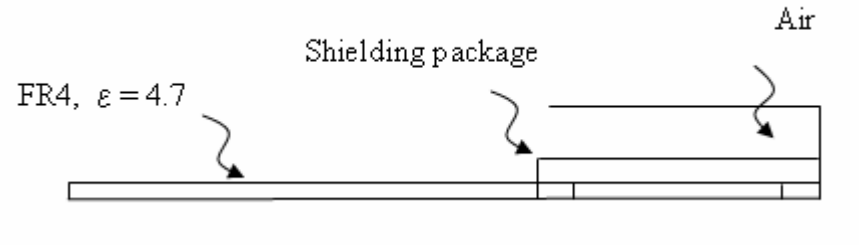

Fig 3-6c

Fig 3-6 Lateral views of the on-package PIFA in air (a) x-y plane (b) x-z plane (c) y-z plane.

The length l and width w of the on-package PIFA determine the resonant frequency, which can be approximated by the formula

$$f_0 = \frac{c}{4(w+l)}$$

where

c is the velocity of light

l and w are the length and width of the radiating element;

f_0 is the resonant frequency.

The radiating element is grounded by a short-circuit strip and fed near the short-circuit strip with the feed line. The input impedance of the antenna can be easily matched to 50Ω by controlling the feed position relative to the short-circuit strip.

The patch size of the antenna is 14.5×15 mm^2 and the height is 2 mm. The short-circuit strip is located on the corner of the patch. The width and height of the shorting strip is 1.5mm and 2mm, respectively. The height and width of the feed line is 3.5 mm and 1.5mm, respectively. The gap between the shorting strip and the feed line is 1mm.

The simulated input return loss and the radiation pattern are shown in Fig 3-7 and Fig 3-8, respectively. It has 150MHz bandwidth from 2.37 to 2.52 GHz when the input return loss is bellow -10dB. The bandwidth can cover IEEE 802.11b/g WLAN band from 2.40 to 2.483 GHz. At x-z plane, the radiation pattern is omnidirectional. The maximum gain and average gain are 4.92dBi and 2.53dBi, respectively. The gains of each plane at 2.45GHz are listed in Table 3-2.

	x-z plane	y-z plane	x-y plane
Maximum Gain	4.92dBi	4.91dBi	2.85dBi
Average Gain	2.53dBi	-1.4dBi	-1.16dBi

Table 3-2 The maximum and average gain of the on-package PIFA in air at 2.45 GHz.

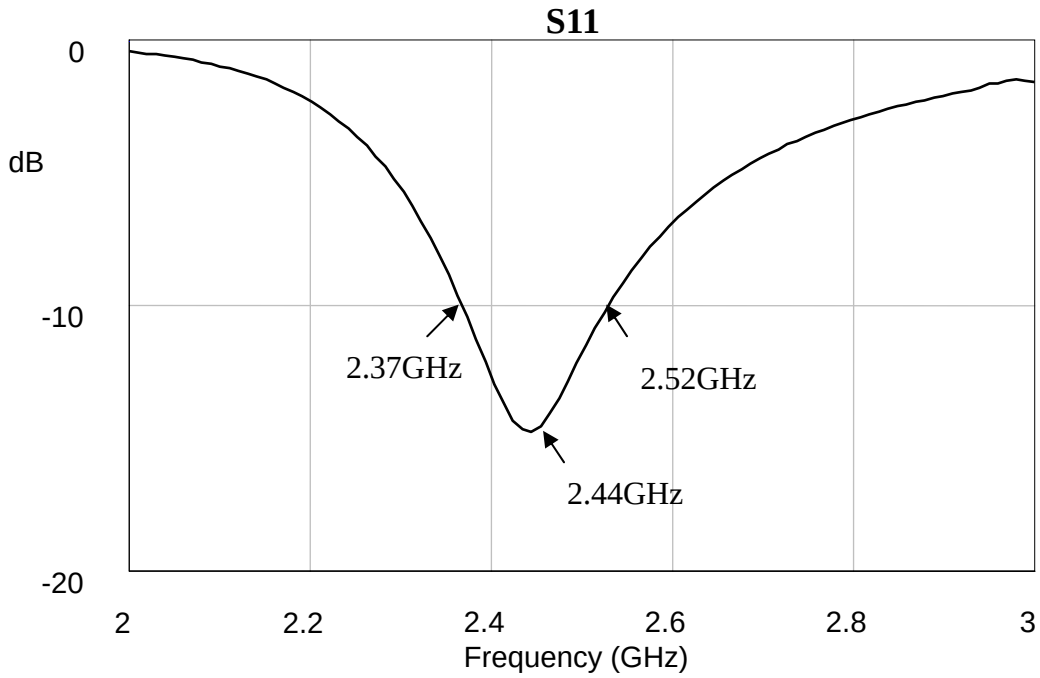

Fig 3-7 Return loss of on-package PIFA in air.

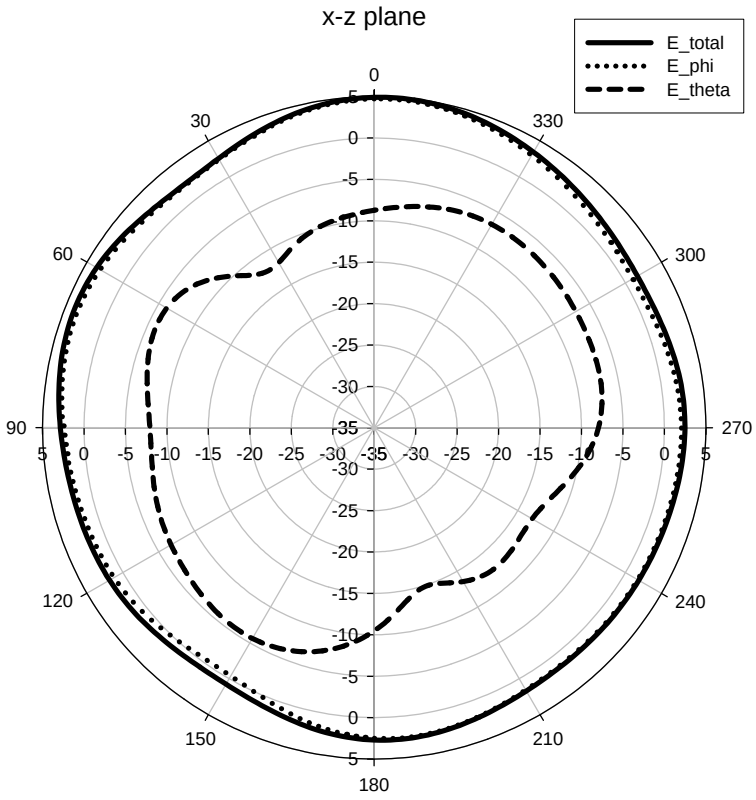

Fig 3-8a Radiation pattern of on-package PIFA in air at x-z plane (2.45GHz).

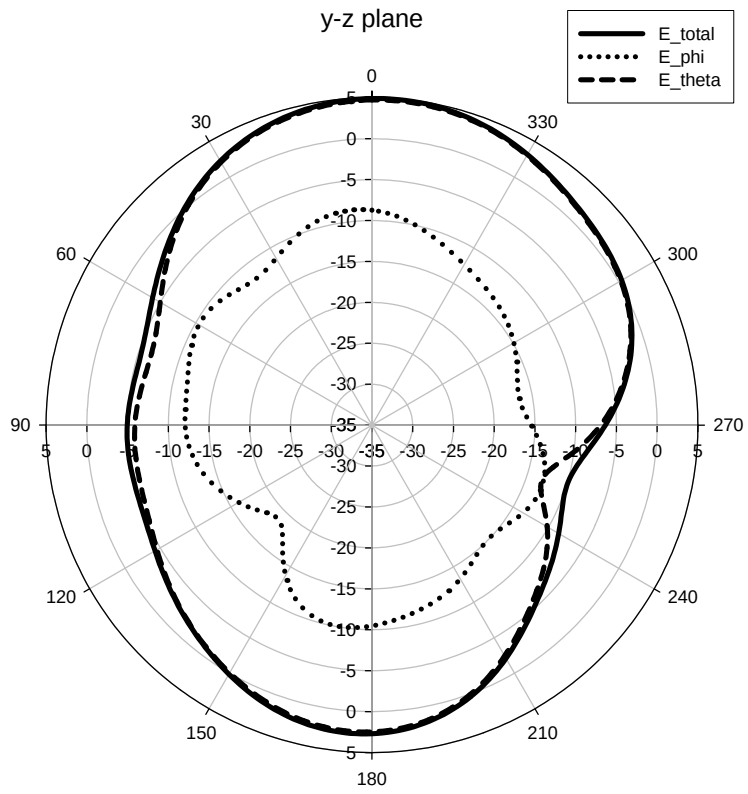

Fig 3-8b Radiation pattern of on-package PIFA in air at y-z plane (2.45GHz).

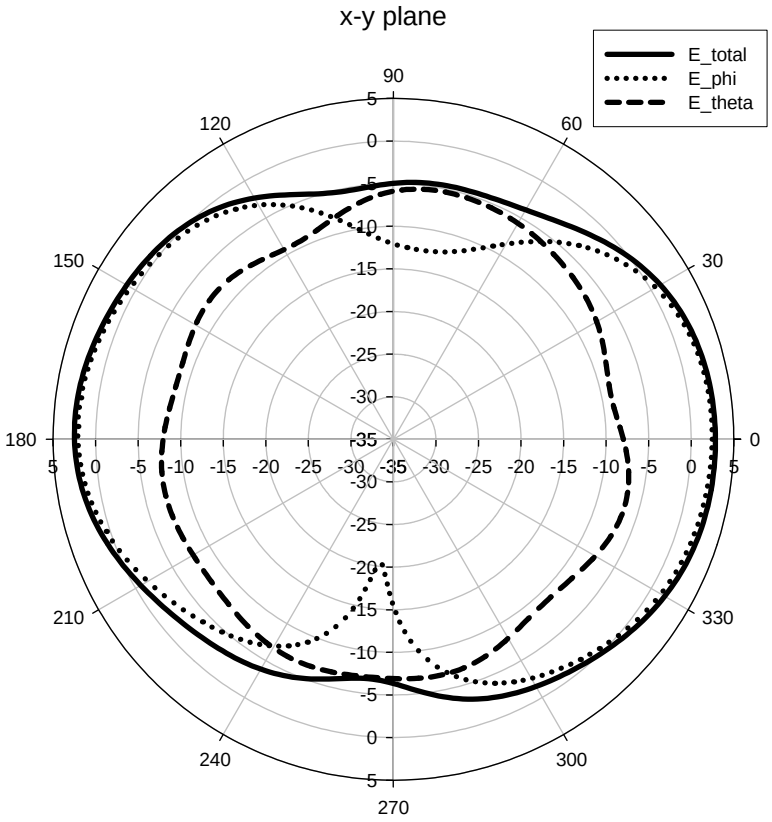

Fig 3-8c Radiation pattern of on-package PIFA in air at x-y plane (2.45GHz).

3.2 Influence of Different Ground Size and Shielding Package

The on-package PIFA in section 3.1.2 is design with the ground size of 20 × 40 mm^2 and the shielding package of 15 ×20 × 1.5 mm^3. The RF components can be placed within the shielding package and the baseband circuits are arranged outside. The ground size and shielding package would be changed when the sizes of circuit components are varied. However, it is well known that the ground size influences the antenna performance and the shielding package is also one part of the on-package PIFA. The change would affect the characteristic of the on-package PIFA. Therefore, we have to investigate the influence of different ground size and shielding package.

3.2.1 Ground Size

The dimensions of the radiating element, the short-citcuit strip and the feed line are fixed and the shielding package is also specified to 15 ×20 × 1.5 mm^3. We alter the ground size to 20 × 35 mm^2, 20 × 45 mm^2, and 20 × 50 mm^2.The input return loss of each case is shown in Fig 3-9. It is observed that the return loss for ground size of 20 × 35 mm^2 and 20 × 45 mm^2 are much poor. The return loss for ground size of 20 × 45 mm^2 has wider bandwidth than the original case. We also compare the radiation patterns of the PIFA with the ground size of 20 × 40 mm^2 and 20 × 45 mm^2. Their patterns are shown in Fig 3-10. The same radiation patterns occur at x-z plane. The patterns at y-z plane are almost the same except at the theta 90 degree and -90degree. The reason is that the ground size of 20 × 45 mm^2 is longer than the order of 20 × 40 mm^2 in the y axis. Therefore, the nulls in the y axis would be more evident. From above discussion, we realize that the structure of the original on-package PIFA do not have not to be redesigned when the ground size varies from 20 × 40 mm^2 to 20 × 45 mm^2.

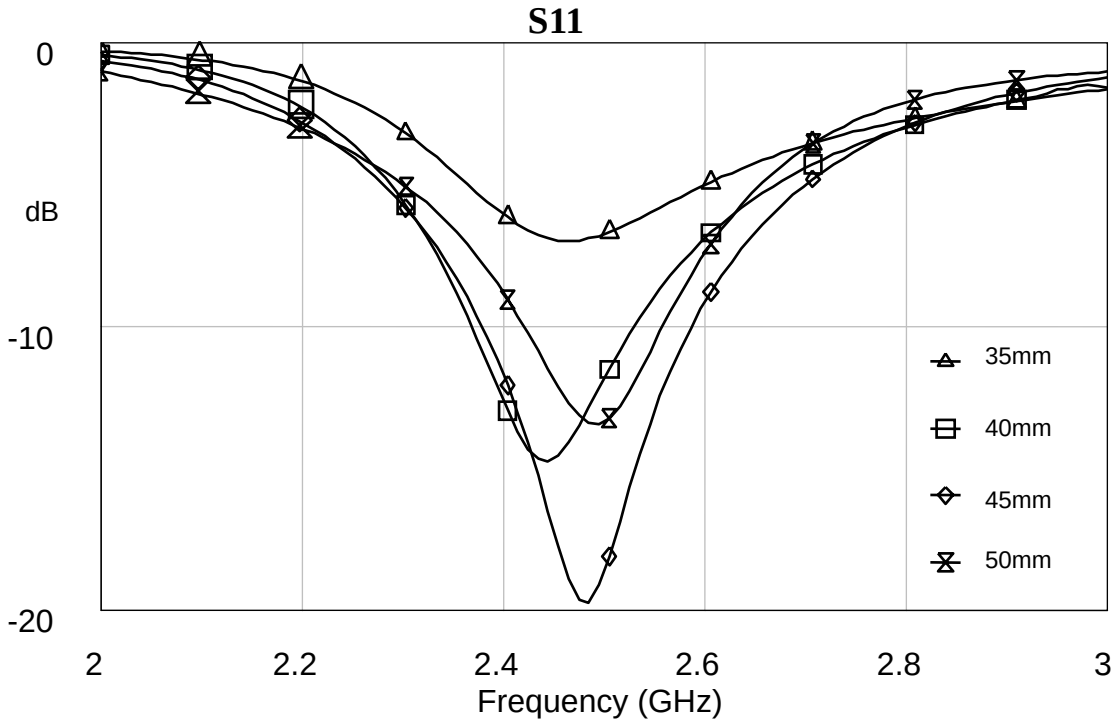

Fig 3-9 Return loss of on-package PIFA with various ground size.

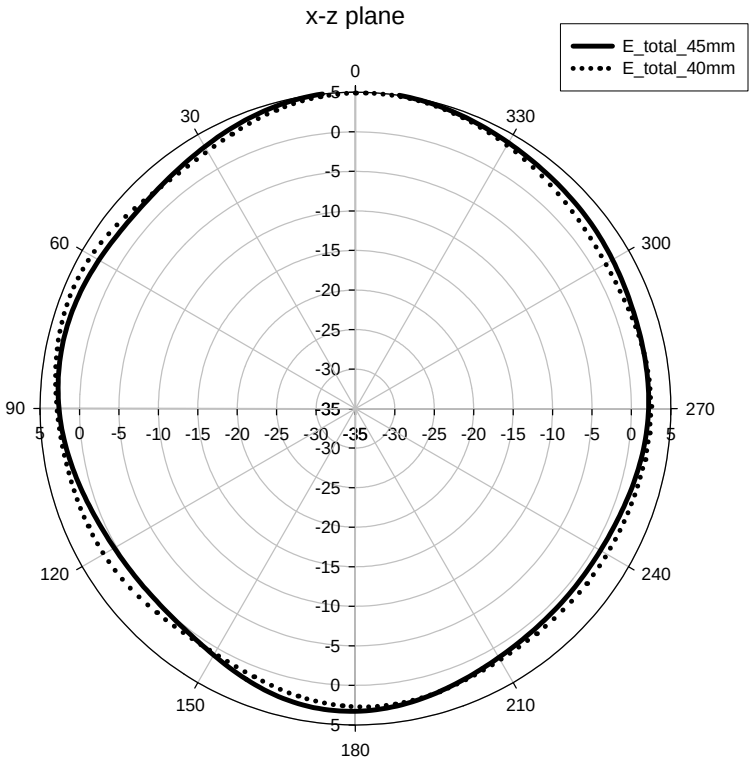

Fig 3-10a Radiation pattern of on-package PIFA with various ground size at x-z plane (2.45GHz)

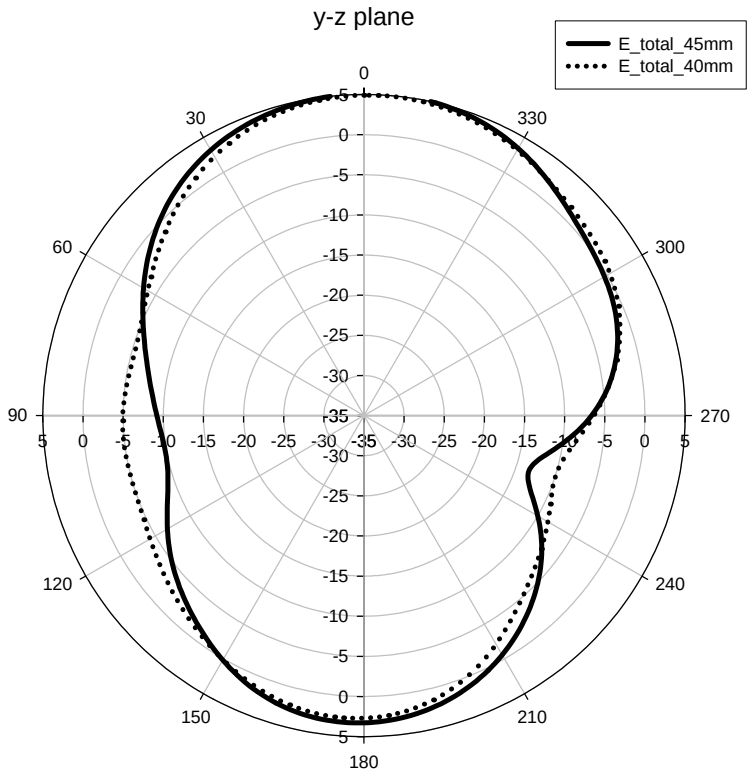

Fig 3-10b Radiation pattern of on-package PIFA with various ground size at y-z plane (2.45GHz).

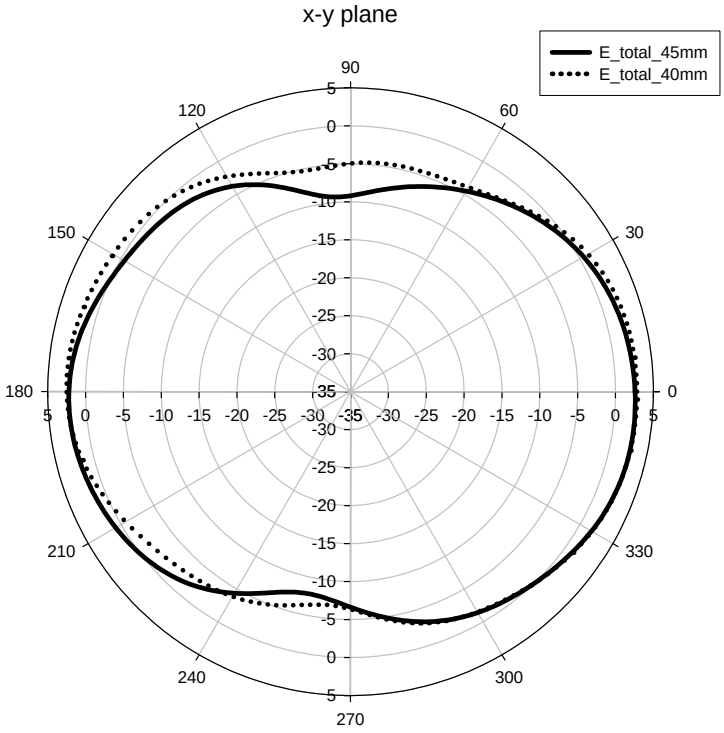

Fig 3-10c Radiation pattern of on-package PIFA with various ground size at x-y plane (2.45GHz).

3.2.2 Shielding Package

The original package size is 20 × 15×1.5 mm ^{3}. In this section, we fix all parameters except for the package size. We change the package size to 15 × 15×1.5 mm ^{3} (case 1), 20 × 20 ×1.5 mm ^{3} (case 2), and 20 × 25×1.5 mm ^{3} (case 3). The simulated return loss is shown in Fig 3-11. It shows the bandwidth of case 1 is wider than the original one, but the other two cases are worst than that. We can see that the change of the package size has less influence than the change of ground size. The radiation patterns of case 1 and original one are both shown in Fig 3-12. The radiation pattern has no difference in any plane. The reason is the package size is less than the ground size which is fixed. We conclude that the configuration of the radiation element do not have not to be redesigned when the package changes from 15 × 15×1.5 mm ^{2} to 15 × 20×1.5 mm ^{3}.

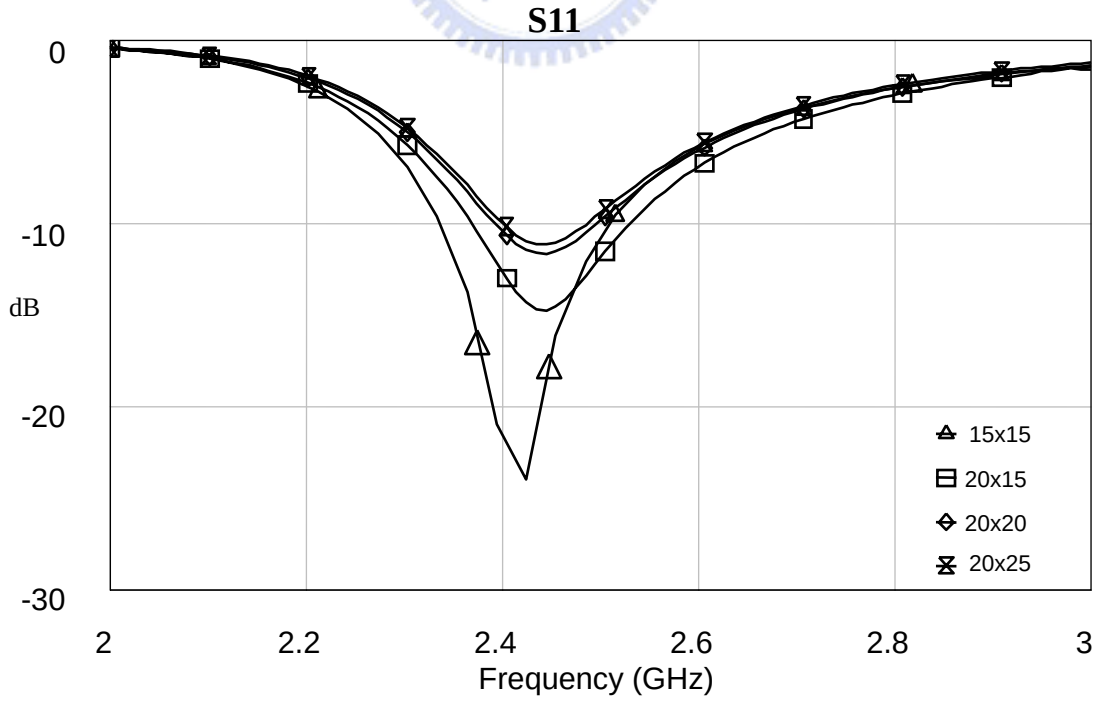

Fig 3-11 Return loss of on-package PIFA with various package size

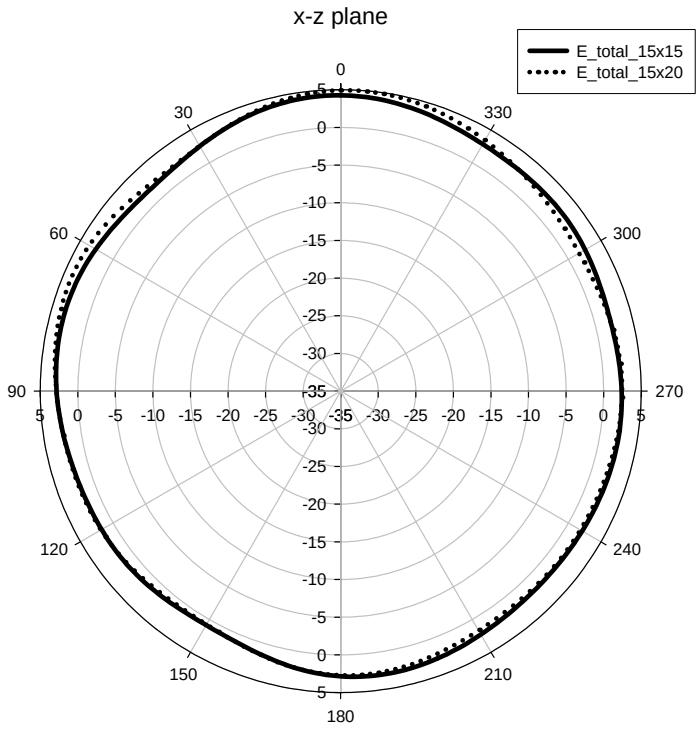

Fig 3-11a Radiation pattern of on-package PIFA with various package size at x-z plane (2.45GHz).

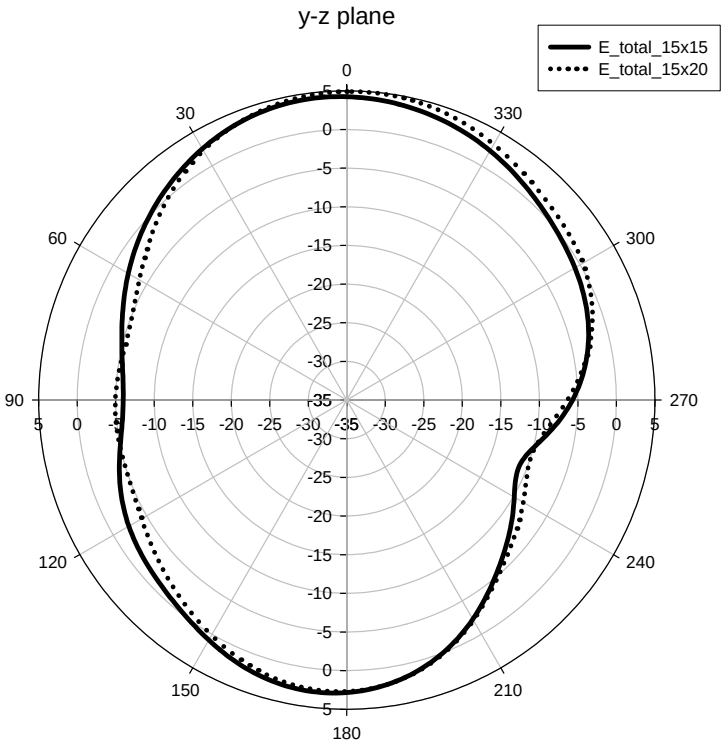

Fig 3-11b Radiation pattern of on-package PIFA with various package size at y-z plane (2.45GHz).

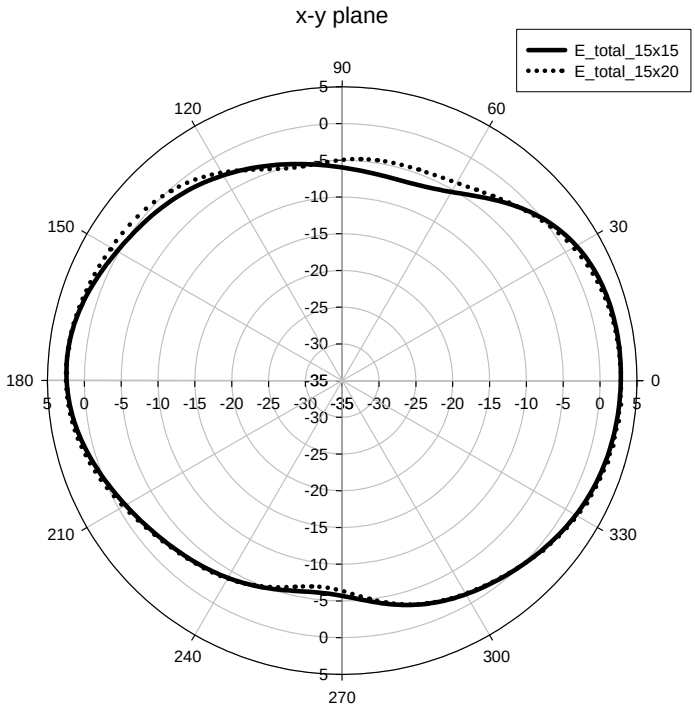

Fig 3-11c Radiation pattern of on-package PIFA with various package size at x-y plane (2.45GHz).

3.3 Measurement

In this section, we carry out the implementation of the on-package PIFA in air, which has been discussed in section 3.1.2, and exhibit the measured results. The on-package PIFA consists of a single folded copper plate, which is shown in Fig 3-12. The upper and the lower palate of the original copper plate are folded as the package part and the patch part of the antenna, respectively. The final folded copper plate is shown in Fig 3-13. The sizes of the package and the radiating element are 15 × 15× 1.5 mm^3 and 14.5 × 17 mm^2, respectively. Fig 3-14 is the photograph of the realized on-package PIFA. The measured bandwidth is 150MHz from 2.37GHz to 2.52 GHz under –10dB return loss, as shown in Fig 3-14. The radiation pattern is also shown in Fig 3-16. The pattern at x-z plane is pretty omnidirectional and the maximum gain and average gain are 1.17 and -0.63dBi, respectively. The gains of all planes at 2.45GHz are listed in Table 3-2. We also investigate the frequency response of the radiation gain at x-z plane as shown in Fig 3-17. The gain has less than 2dBi variation centered at 0dBi. This on-package PIFA hold an excellently linear frequency response.

	x-z plane	y-z plane	x-y plane
Maximum Gain	1.17dBi	3.09dBi	0.61dBi
Average Gain	-0.63dBi	-2.78dBi	-3.17dBi

Table 3-3 Measured maximum and average gain of the on-package PIFA at 2.45 GHz.

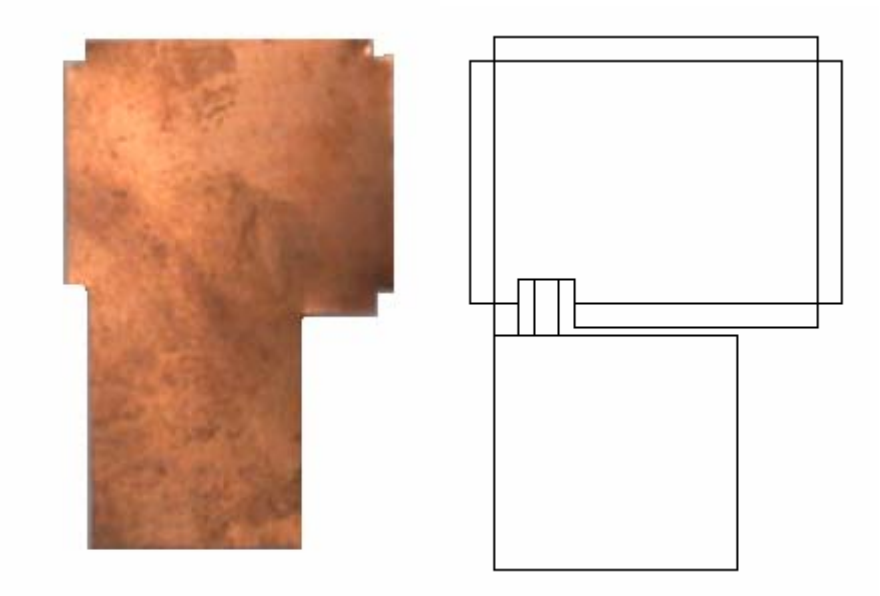

Fig 3-12 The original copper plate.

Fig 3-13 The folded copper plate.

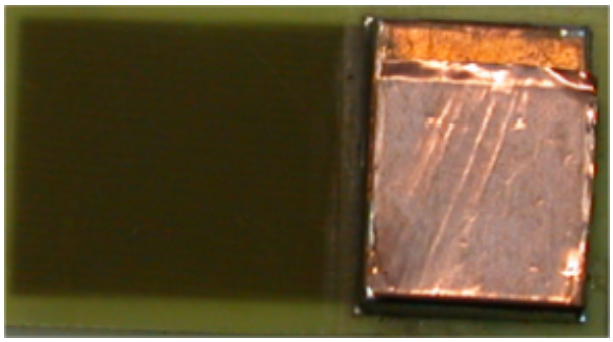

Fig 3-14 Photograph of implemented antenna.

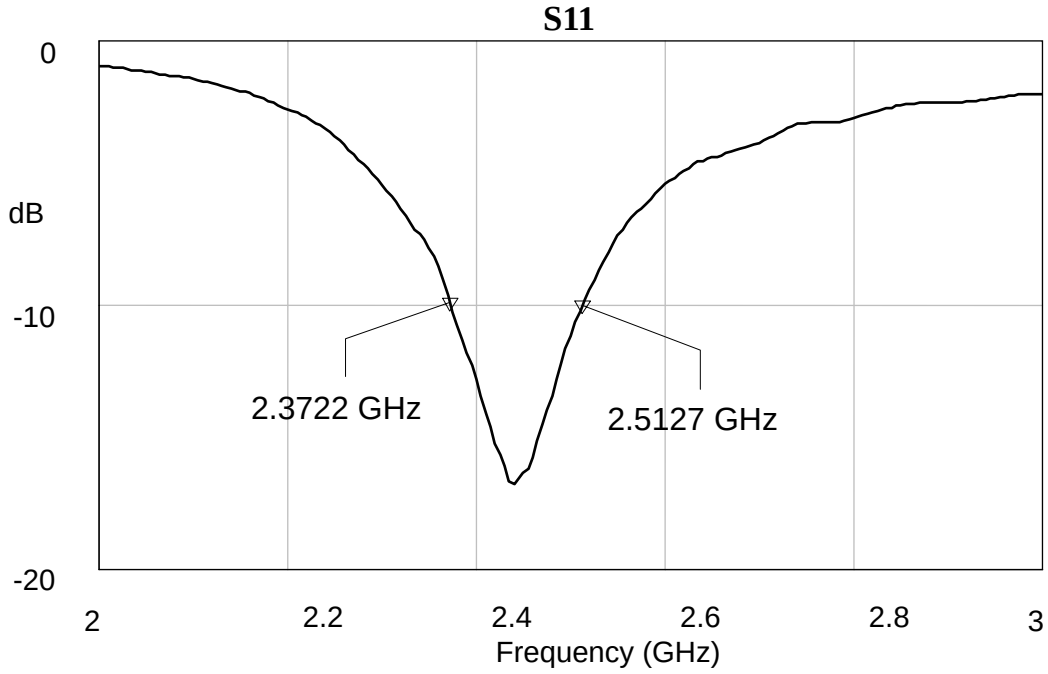

Fig 3-15 Measured return loss of the on-package PIFA.

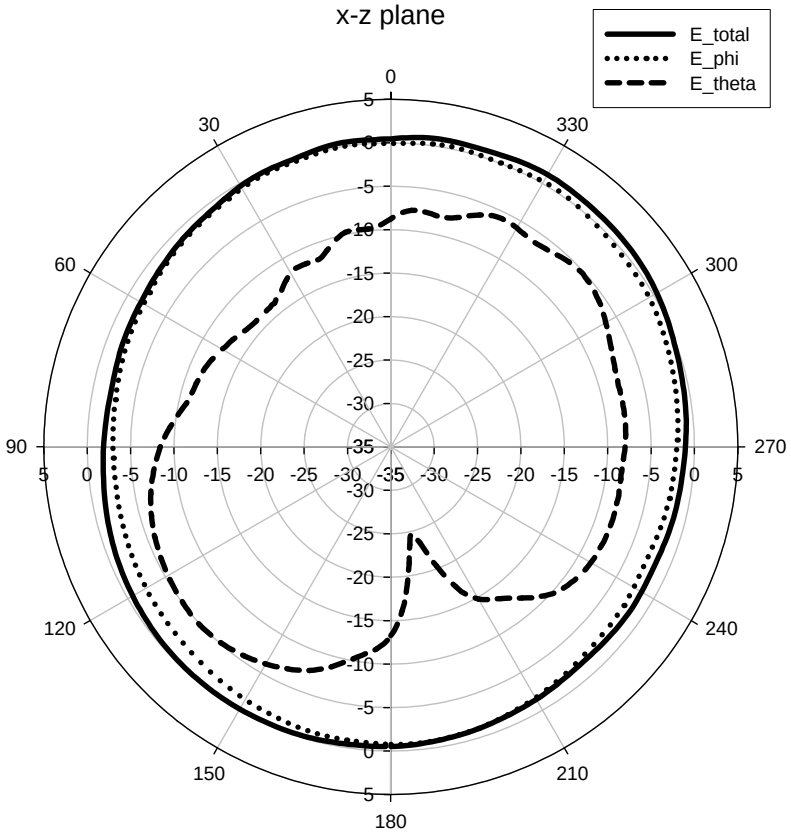

Fig 3-16a Measured radiation pattern of the on-package PIFA at x-z plane (2.45GHz).

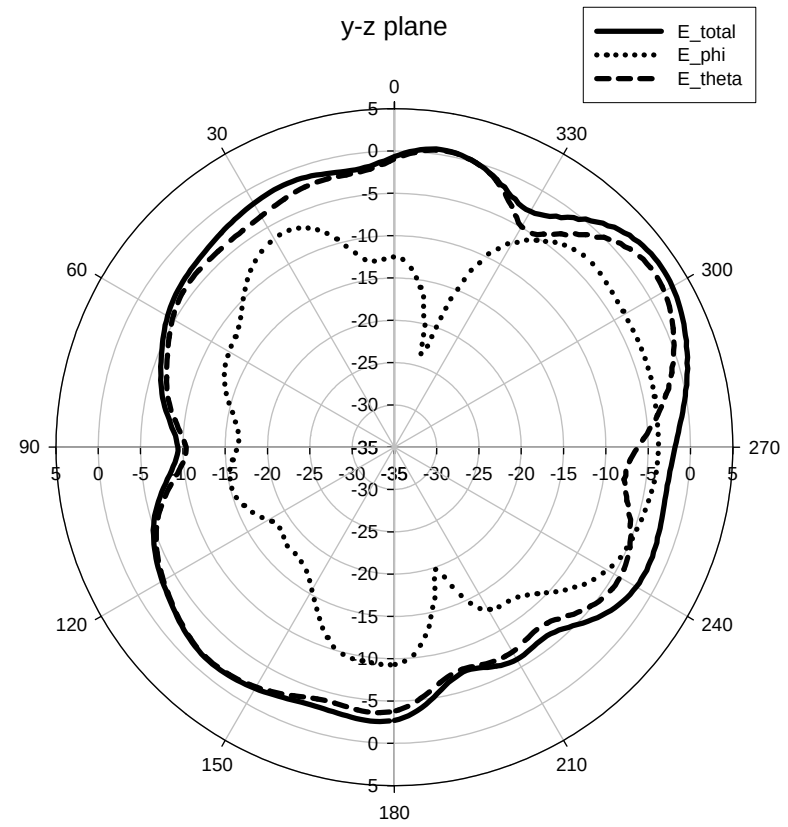

Fig 3-16b Measured radiation pattern of the on-package PIFA at y-z plane (2.45GHz).

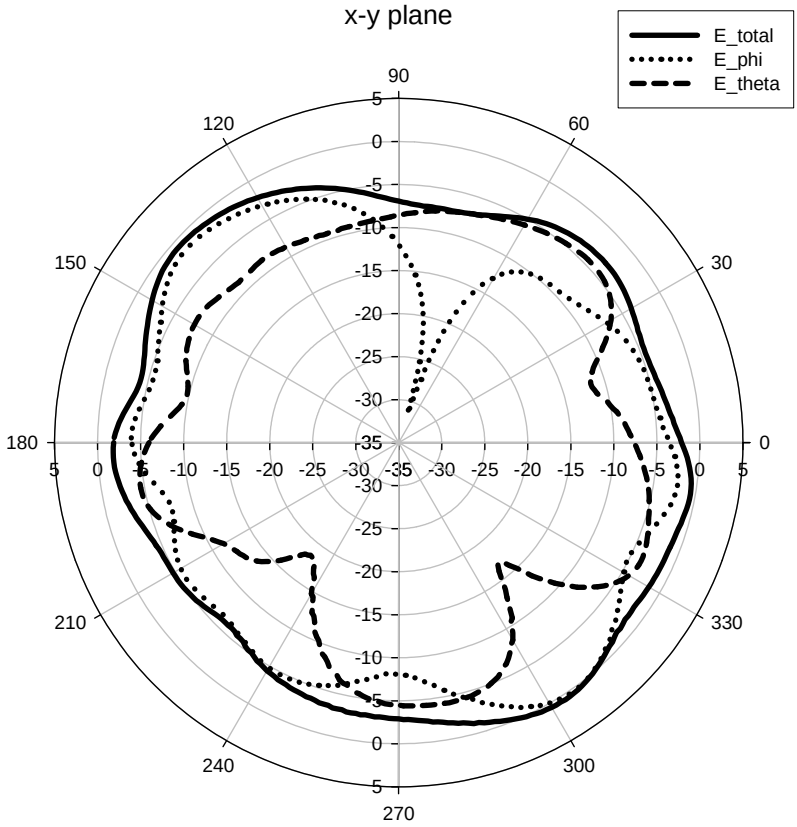

Fig 3-16c Measured radiation pattern of the on-package PIFA at x-y plane (2.45GHz).

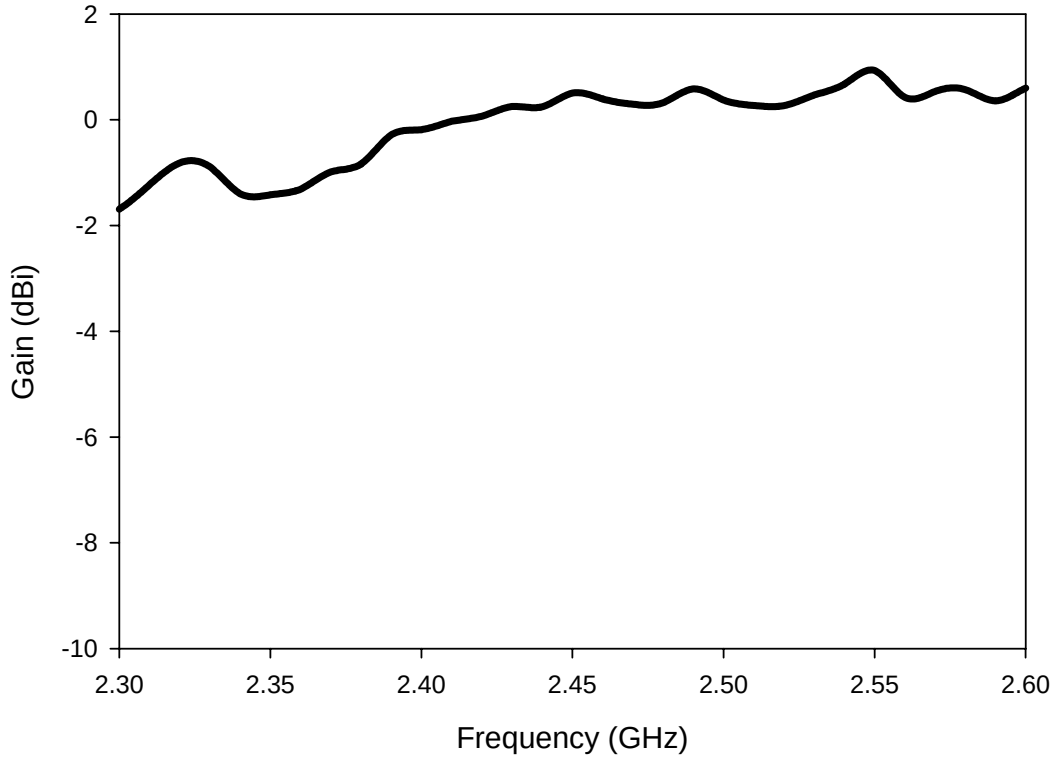

Fig 3-17 Gain vs. Frequency characteristic of the on-package PIFA at x-z plane (2.45GHz).

Chapter 4

Coupling between On-Package PIFA and RF Components

4.1 Characteristic of LTCC BPF

Basically, WLAN RF circuits consist of an antenna, a T/R switch, filters, mixers, voltage-control oscillators, a low-noise amplifier, and a power amplifier [13]-[15]. The switch is set up for TX or RX path with appropriate bias. On RX path, the band-pass filter for band selection is followed by a low-noise amplifier. The RF signal amplified by the PA radiates through an antenna when the switch is set up for the TX path. The low-pass filter can suppress the output harmonics of the PA. Among these components, the low-pass filter, the band-pass filter and the matching network of the amplifiers are all passive components. The coupling effect between the on-package PIFA and the RF passive components in the shielding package can be investigated by the 3-D full-wave EM simulator Ansoft HFSS 8.0. We select a BPF to represent the passive components which are formed with inductors and capacitors.

The band-pass filter LTB-2520-2G4H3-A2 is designed via low-temperature co-fired ceramic (LTCC) technology by MAG.. LAYERS Scientific-Technology Co., LTd. Fig 4-1 shows the top-view of the LTCC BPF with the size of $2.5\times2.0\times1\ mm^3$. More detailed dimensions are also shown in Fig 4-1.The pass band is 100MHz from 2400 to 2500 MHz. The maximum insertion loss is 2.0dB. Table 4-2 shows the detailed electrical specifications and Fig 4-5 indicates the electrical characteristic which is measured by Aglient E5071A Network Analyzer. The measured insertion loss is -1.5dB. The above characteristic is obtained from the datasheet of the BPF.

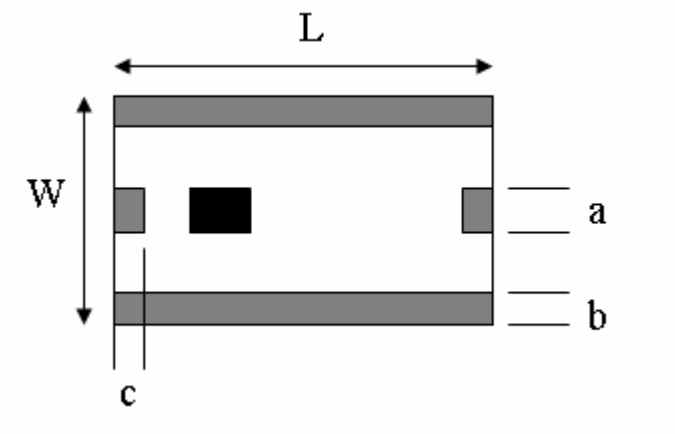

L	2.5±0.20 mm
W	2.0±0.20 mm
T	1.0±0.15 mm
a	0.50±0.20 mm
b	0.30±0.15 mm
c	0.30±0.15 mm

Fig 4-1 Top view and dimensions of the LTCC BPF (2520)

Electrical Specifications		TEST INSYRUMENT: AGLIENT E5071A NETWORK ANALYZER
Pass Band	2400-2500 MHz	
Insertion loss in BW	2.0 dB max	
Return loss	10 dB min	
Impedance	50 ohms	
Attenuation	30dB min at 880-915MHz	
	30dB min at 1710-1785 MHz	
	28dB min at 1850-1910 MHz	
	25dB min at 4800-5000 MHz	

Table 4-1 Electrical specifications of the LTCC BPF (2520)

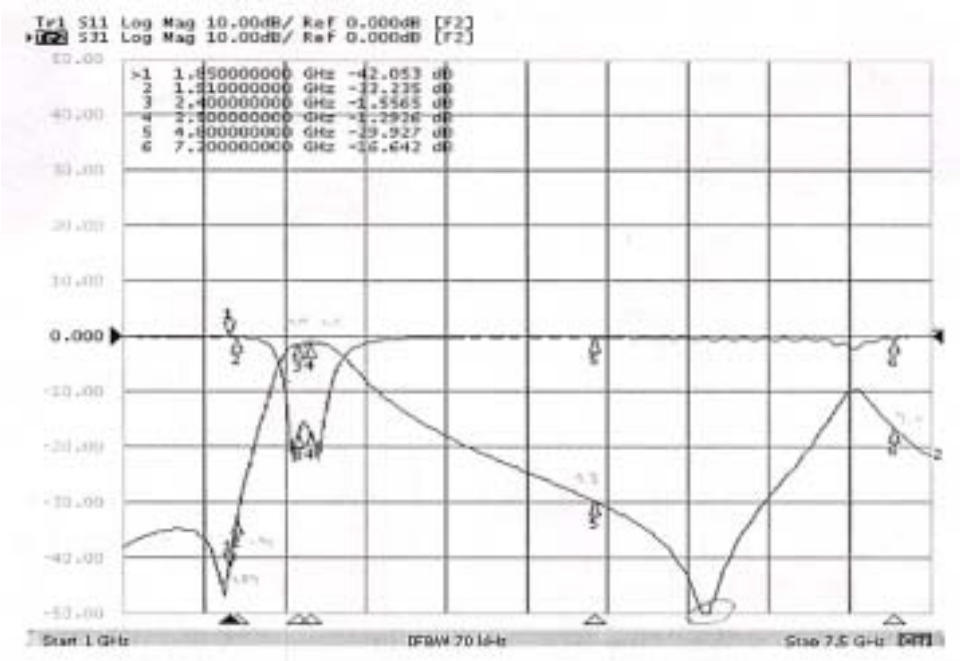

Fig 4-2 Electrical Characteristic of the LTCC BPF (2520)

4.2 Coupling between On-Package PIFA and LTCC BPF

In this section, we investigate the coupling effect between the on-package PIFA and LTCC BPF [16]. We place a band-pass filter LTB-2520-2G4H3-A2 in the shielding package, which is one part of the on-package PIFA. We have the BPF to be arranged at six different positions in the package to observe the phenomenon. Fig 4-3 shows the diagram of the BPF arranged at different positions. The six cases are represented as case A, case B, case C, case D, case E, and case F. In case A, the BPF is arranged 1 mm apart from the input of the antenna. The BPF is also moved backward 5 mm from position A in case B. In case C, the BPF has 13 mm right-shift from the position A. In case D, the BPF has 13 mm right-shift from the position B. The BPF is arranged at the center of the package in case E. Finally, the BPF is rotated by -90 degree in case F. Port 1 and port 2 are the input and output of BPF, respectively, and the input of the antenna is port 3. We simulate these cases by 3-D full-wave EM simulator Ansoft HFSS 8.0. The performances in each case are also compared with that the original BPF and the on-package PIFA.

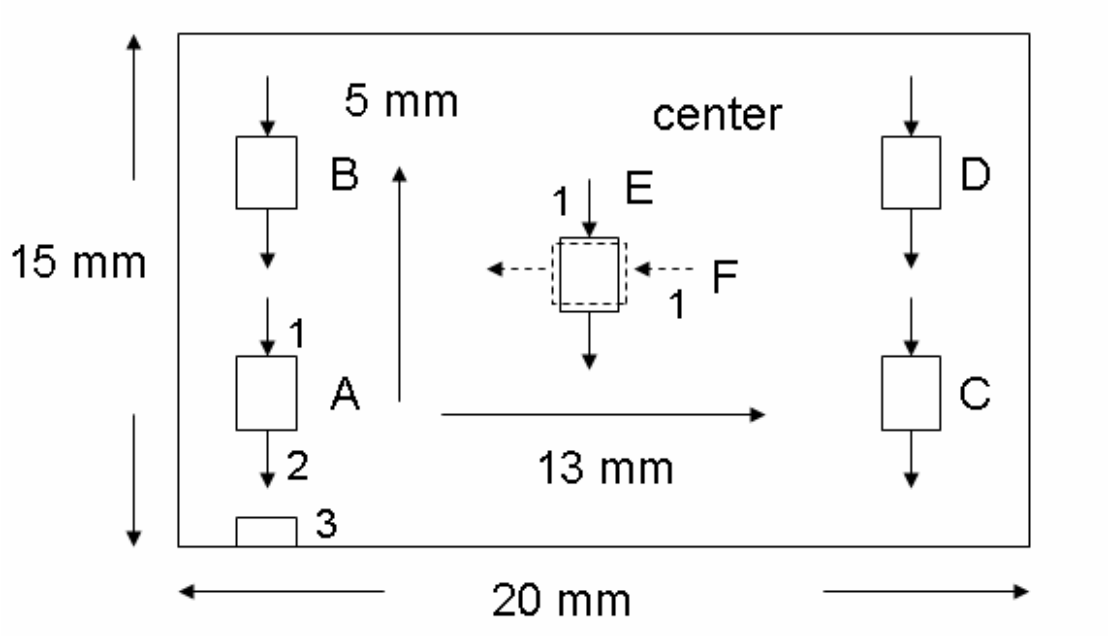

Fig 4-3 The diagram of the BPF arranged at different positions.

Fig 4-4 shows the input return loss in each case. The input return loss has merely change wherever the BPF is arranged. The insertion loss in each case is shown in Fig 4-5. Fig 4-5 shows that the insertion loss is not influenced except for the high frequency transmission zero. The insertion loss in the pass band is less than -2dB. The reason for the variation of the transmission zero is that the designed transmission zero is seriously influenced by the parasitic inductance [17]. Fig 4-6 shows the return loss of the on-package PIFA in each case and the return loss also has merely change. In Fig 4-7 and Fig 4-8, the isolation of S13 and S23 are at more than 30dB in WLAN band. The isolation between the antenna and BPF has a better performance when the BPF is apart from the feed point of the antenna.

We also connect the input of the on-package PIFA to the output of BPF when the BPF is arranged at the position B. Fig 4-9 shows the input return loss of the BPF. The return loss has an additional null due to the on-package PIFA. The new radiation pattern is also compared with the original on-package PIFA as shown in Fig 4-10. The shape of radiation pattern has merely change, and the gain is around 1.5dBi lower than that of original on-package PIFA due to the insertion loss of the BPF. The gains of all planes are listed in Table 4-2 and those of the original on-package PIFA are also listed in Table 4-3.

	x-z plane	y-z plane	x-y plane
Maximum Gain	3.39dBi	3.25dBi	1.40dBi
Average Gain	1.14dBi	-2.90dBi	-2.62dBi

Table 4-2 The maximum and average gain of the on-package PIFA with BPF at the position B at 2.45GHz.

	x-z plane	y-z plane	x-y plane
Maximum Gain	4.92dBi	4.91dBi	2.85dBi
Average Gain	2.53dBi	-1.4dBi	-1.16dBi

Table 4-3 The maximum and average gain of the original on-package PIFA at 2.45GHz.

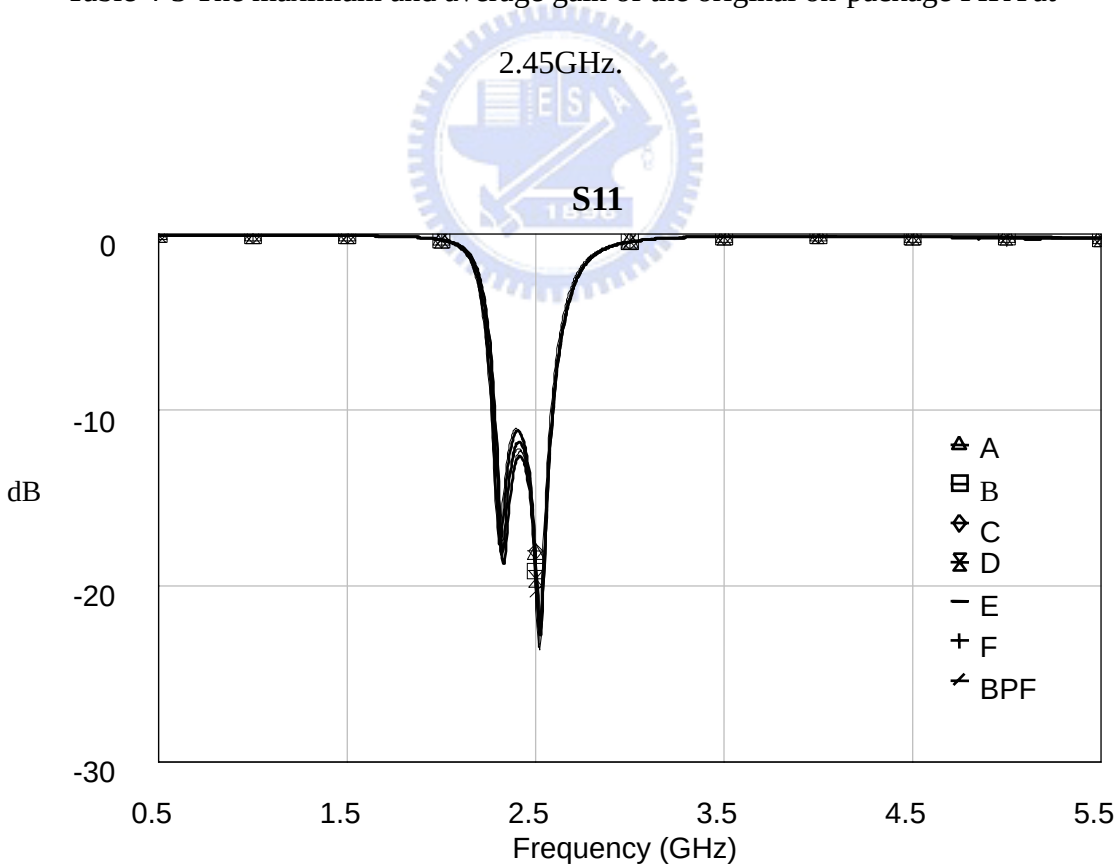

Fig 4-4 Return loss of the BPF in all cases.

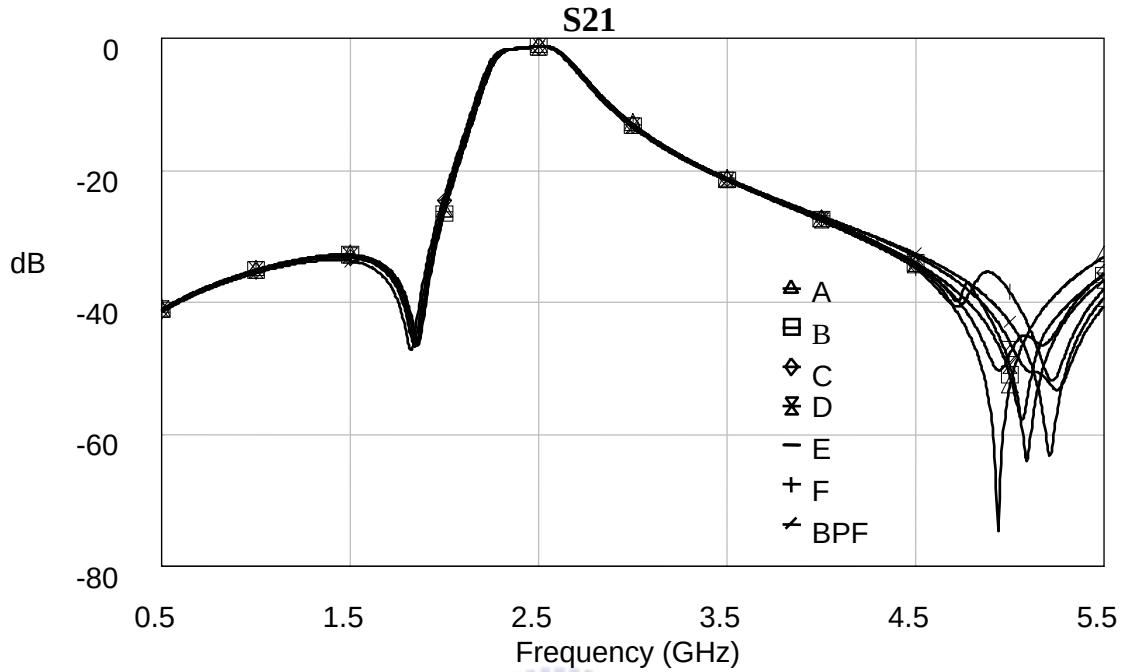

Fig 4-5 Insertion loss of the BPF in all cases.

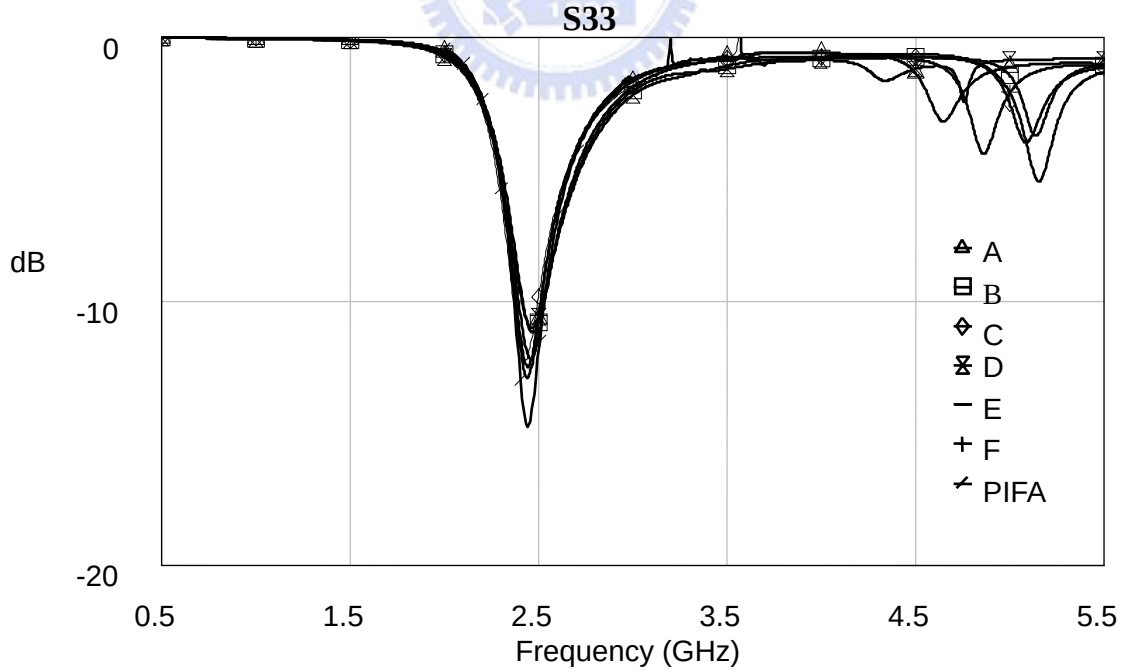

Fig 4-6 Return loss of the on-package PIFA in all cases.

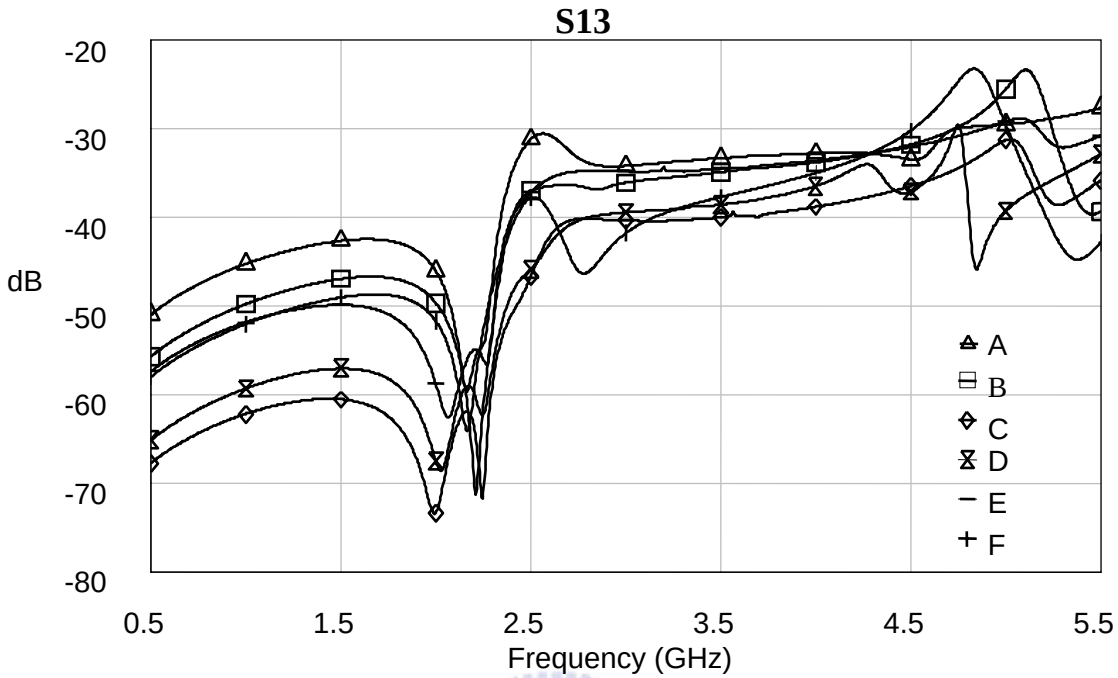

Fig 4-7 Isolation of S13 in all cases.

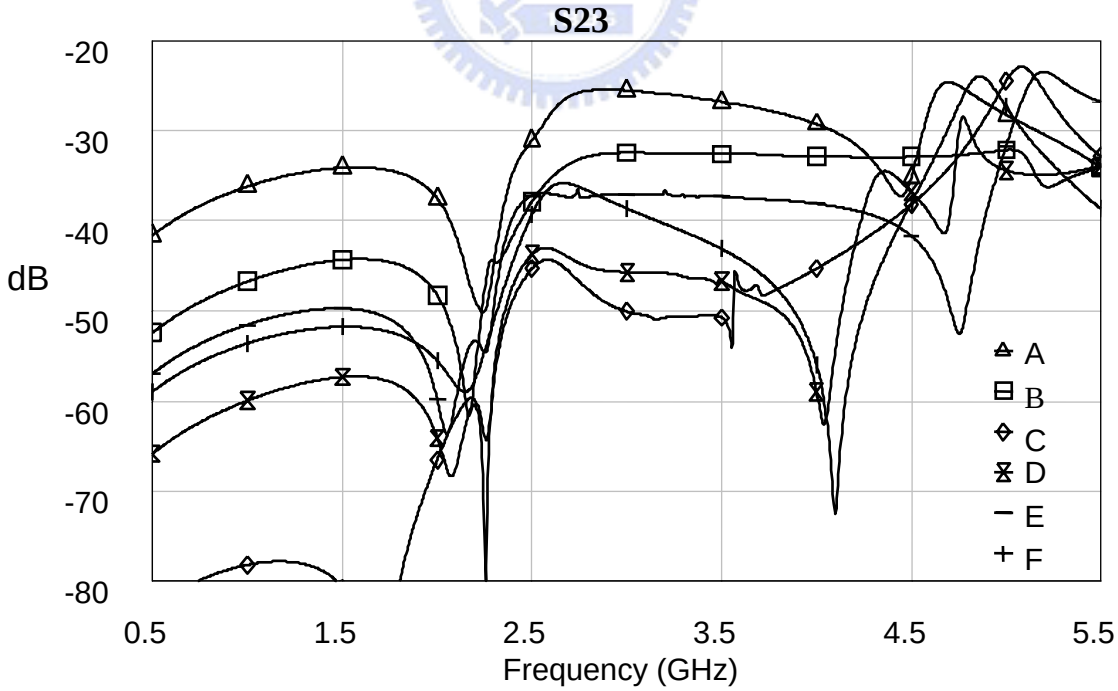

Fig 4-8 Isolation of S23 in all cases.

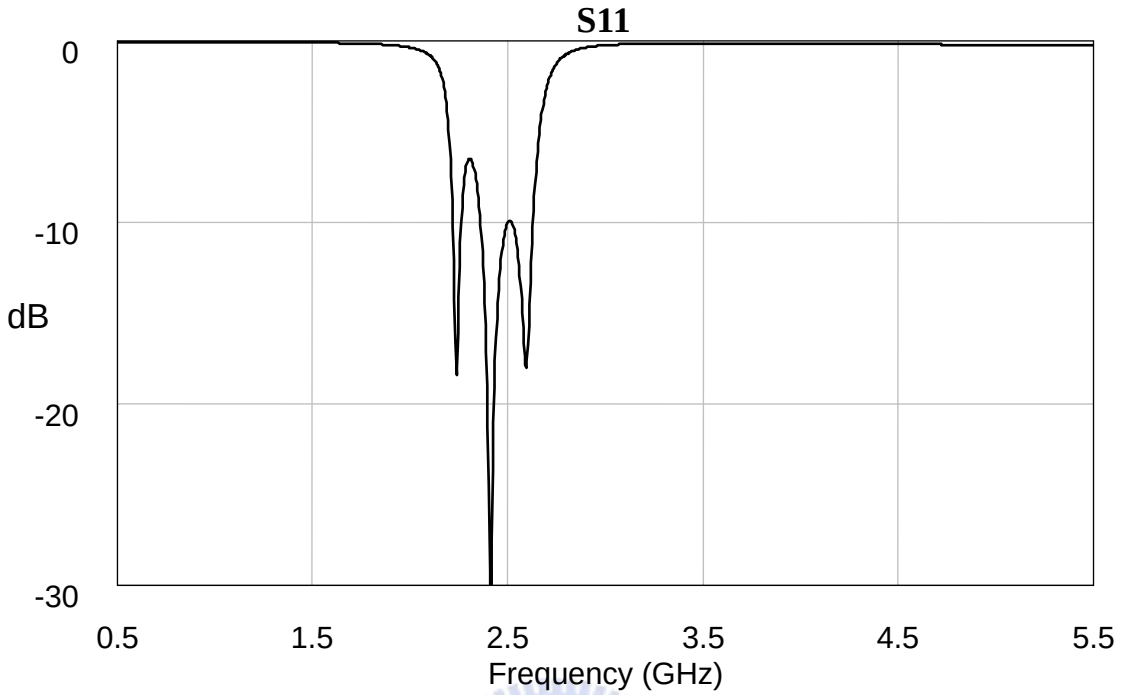

Fig 4-9 Return loss of the BPF with on-package PIFA.

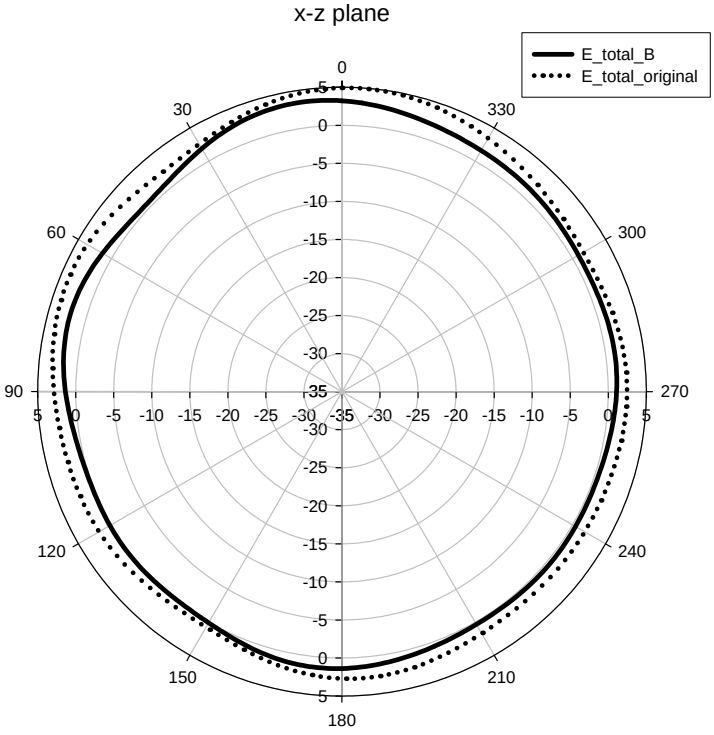

Fig 4-10a Radiation pattern of the on-package PIFA with and without BPF at x-z plane (2.45GHz).

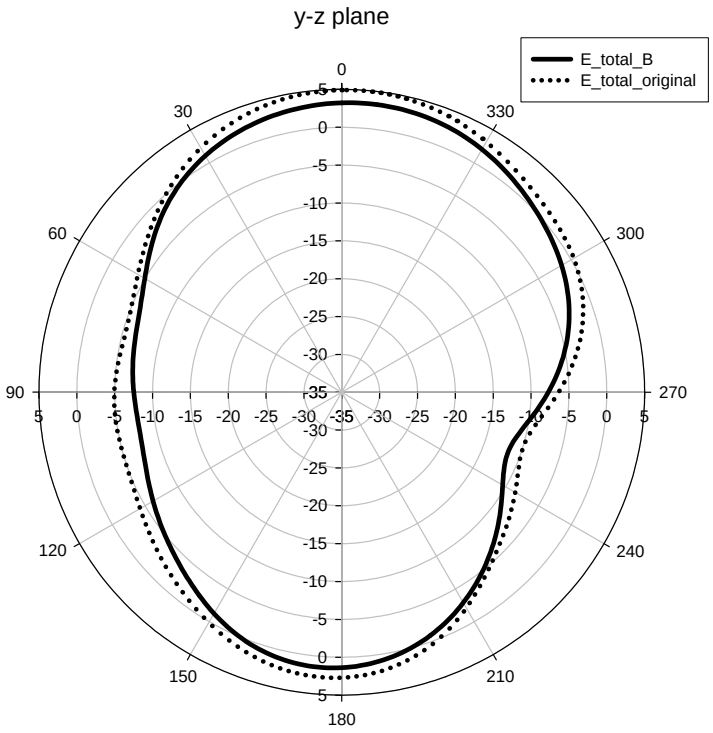

Fig 4-10b Radiation pattern of the on-package PIFA with and without BPF at y-z plane (2.45GHz).

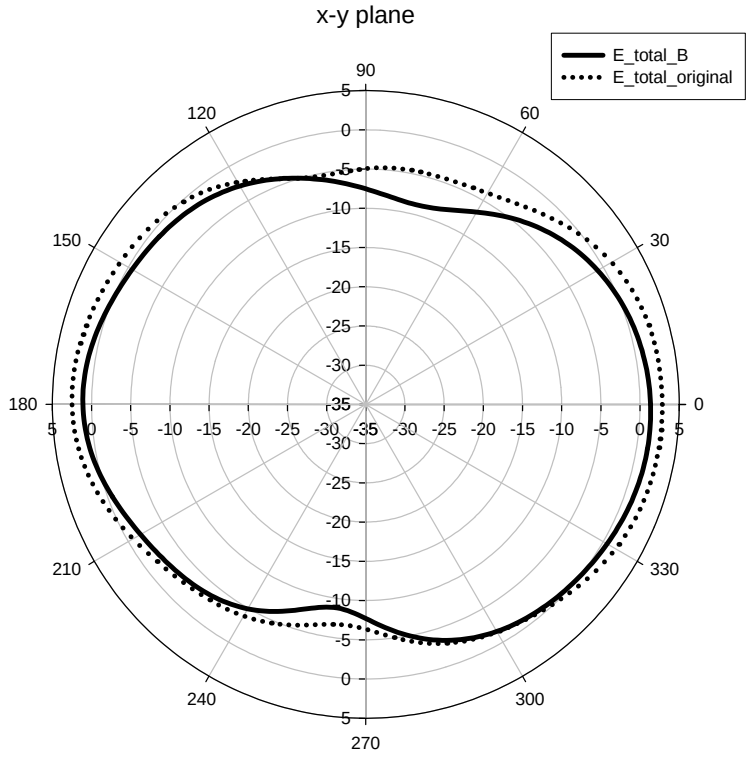

Fig 4-10c Radiation pattern of the on-package PIFA with and without BPF at x-y plane (2.45GHz).

4.3 Measurement

In this section, we verify the characteristic of the LTCC BPF and the coupling effect between on-package PIFA and LTTC BPF in case A , B and F, which has been discussed in section 4.2. Fig 4-11 shows the photograph of the LTCC BPF. The photographs of on-package PIFA with BPF in case A and F are shown in Fig 4-12a and 4-12b, respectively. In Fig 4-13, the photograph of on-package PIFA connected to BPF at the position B is shown.

The measured return loss and insertion loss are shown in Fig 4-14 and the insertion loss is 1.54dB in WLAN band. We calibrate the connector loss and microstrip-line loss by TRL calibration. It is observed that the measured characteristic is very identical to the datasheet except for the high frequency transmission zero caused by the parasitic inductance. The PCB board we adopted is 0.8mm FR4, which is thicker than the test kit. Therefore, the parasitic inductance is larger than the original one.

In Fig 4-15, we observe that the return loss has merely change wherever the BPF is arranged at the position A or F. Fig 4-16 shows the measured insertion loss in case A and F. The difference of the insertion loss between the case F (or A) and the original one is mainly caused by the coaxial-line loss and the discontinuity. The loss of coaxial lines and the discontinuity is around 1dB, as shown in Fig 4-17. Therefore, the insertion loss in both case A and F is about 1.8dB. Fig 4-18 indicates that the return loss of on-package PIFA in case A and F is merely changed. The characteristic of BPF and on-package PIFA is not changed in both cases. The isolation between antenna and BPF has a better performance when the BPF is arranged at the position F than the position A, as shown in Fig 4-19 and 4-20. The reason is that the position F is more far away from the feed point of the antenna. Nevertheless, the isolation of S23 is

worse than that of S13 because the output of the BPF is closer to the feed point of the antenna.

The input of the on-package PIFA is connected to the output of the BPF when the BPF is arranged at the position B. The return loss has an extra null due to the on-package PIFA, as shown in Fig 4-21. The measured radiation pattern is similar to the original on-package PIFA, as shown in Fig 4-22 and the gain reduction is caused by the insertion loss of the BPF and the error in measurement process. The gains of E total at all planes are listed in Table 4-4 and those of the original on-package PIFA are also listed in Table 4-5. Fig 4-23 shows that the frequency response of the BPF occurs in the radiation gain of E phi at x-z plane.

	x-z plane	y-z plane	x-y plane
Maximum Gain	-1.34dBi	1.68dBi	-1.3dBi
Average Gain	-3.38dBi	-5.30dBi	-5.12dBi

Table 4-4 Measured maximum and average gain of the on-package PIFA with BPF at the position B at 2.45 GHz.

	x-z plane	y-z plane	x-y plane
Maximum Gain	1.17dBi	3.09dBi	0.61dBi
Average Gain	-0.63dBi	-2.78dBi	-3.17dBi

Table 4-5 Measured maximum and average gain of the original on-package PIFA at 2.45 GHz.

Fig 4-11 Photograph of LTCC BPF.

Fig 4-12a Photograph of on-package with BPF in case A.

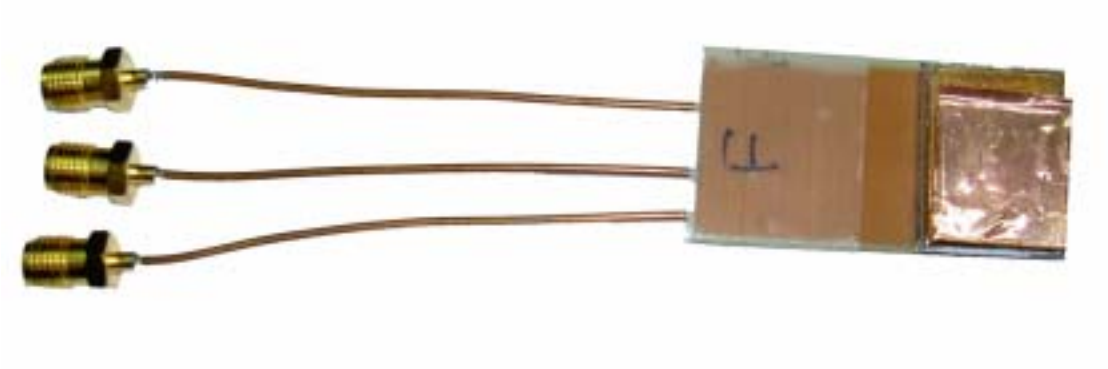

Fig 4-12b Photograph of on-package PIFA in case F.

Fig 4-13 Photograph of on-package PIFA connected to BPF at the position B.

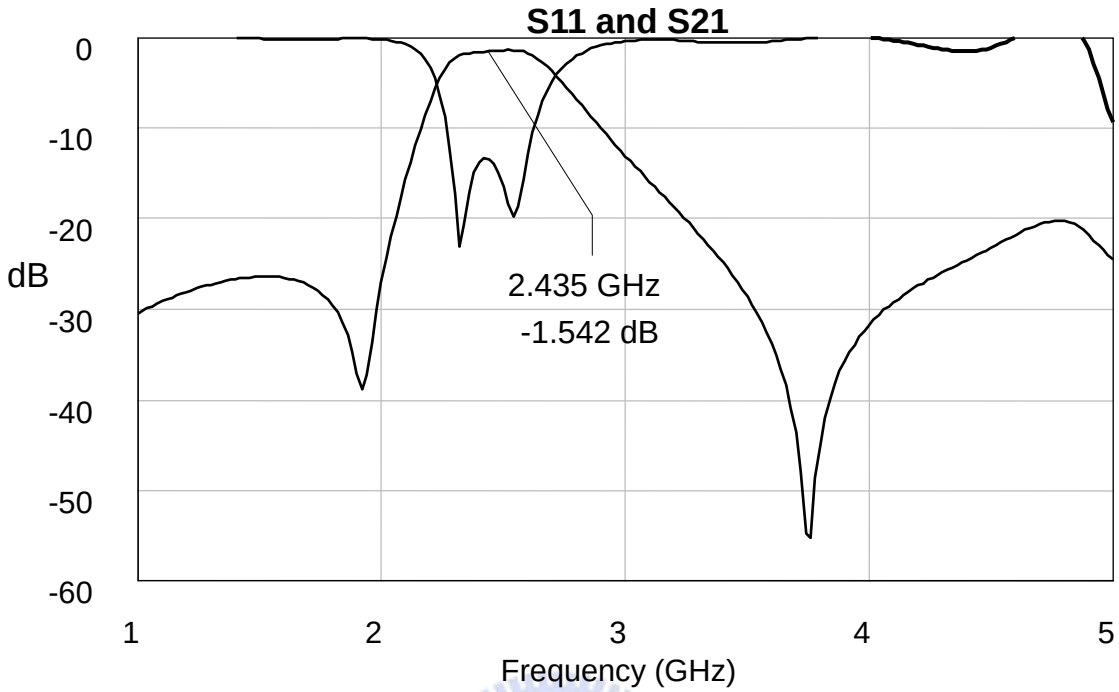

Fig 4-14 Measured return loss and insertion loss of the LTCC BPF.

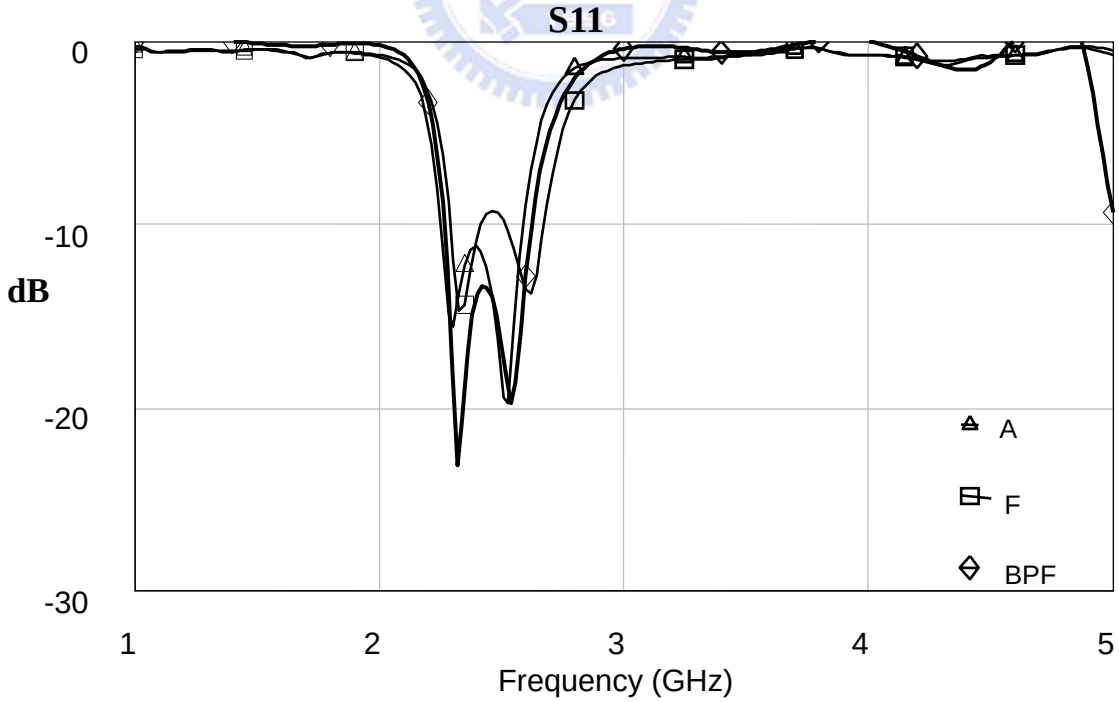

Fig 4-15 Measured return loss of the BPF in case A and F.

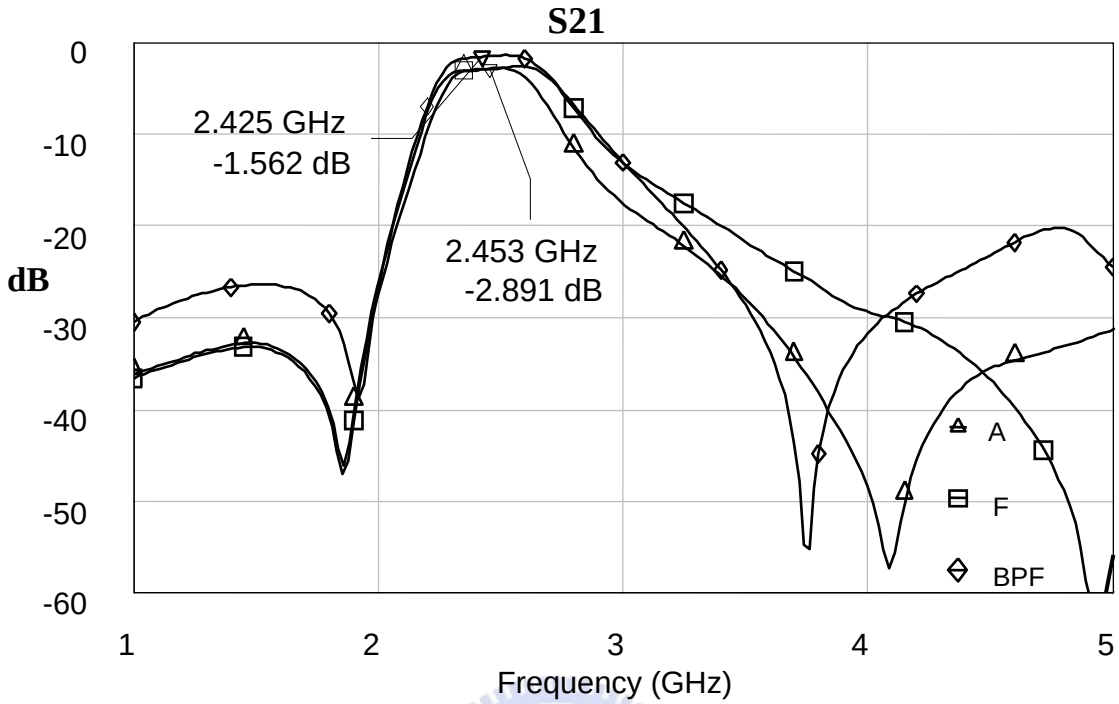

Fig 4-16 Measured insertion loss of the BPF in case A and F.

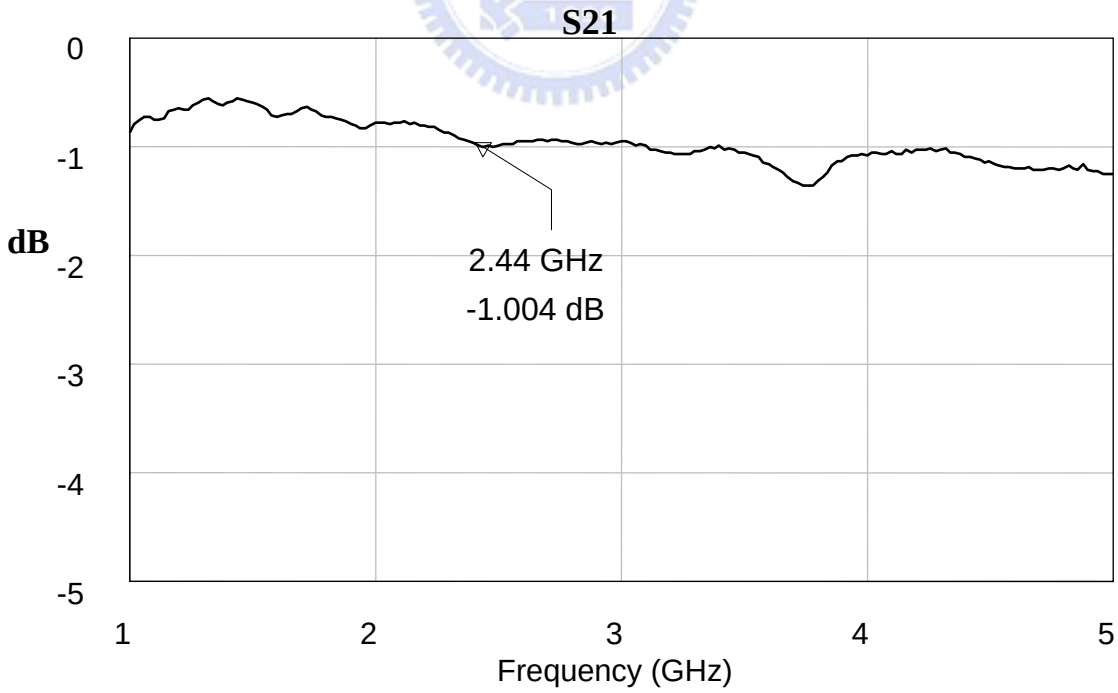

Fig 4-17 Loss due to the coaxial lines and discontinuity

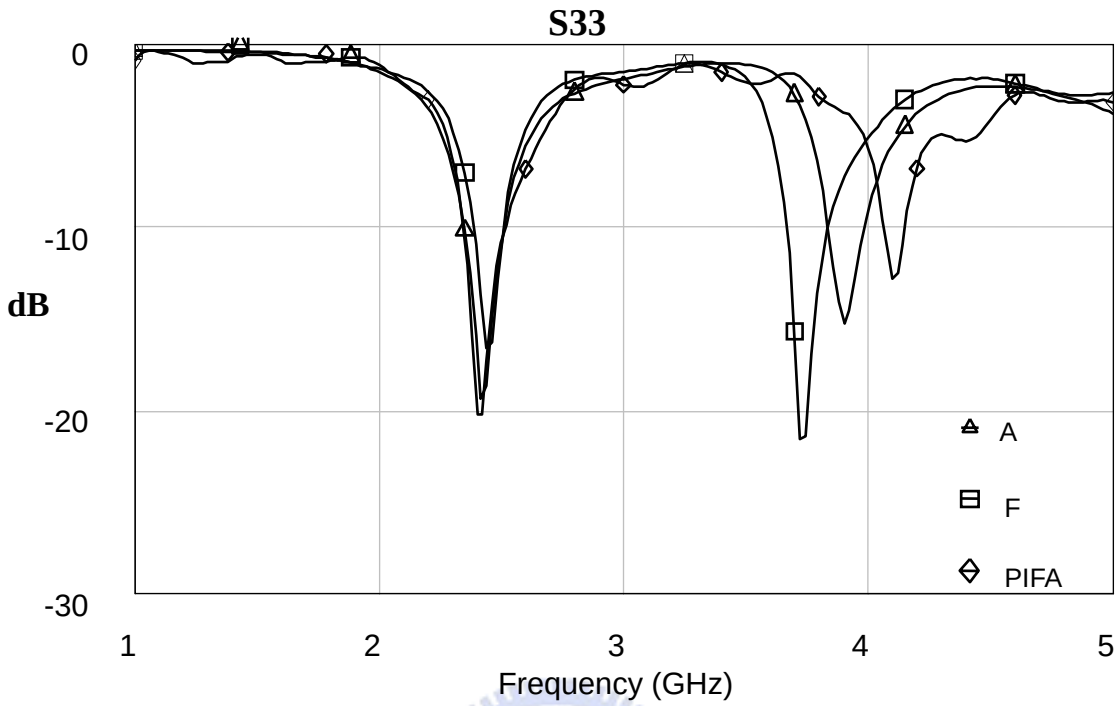

Fig 4-18 Measured return loss of on-package PIFA in case A and F.

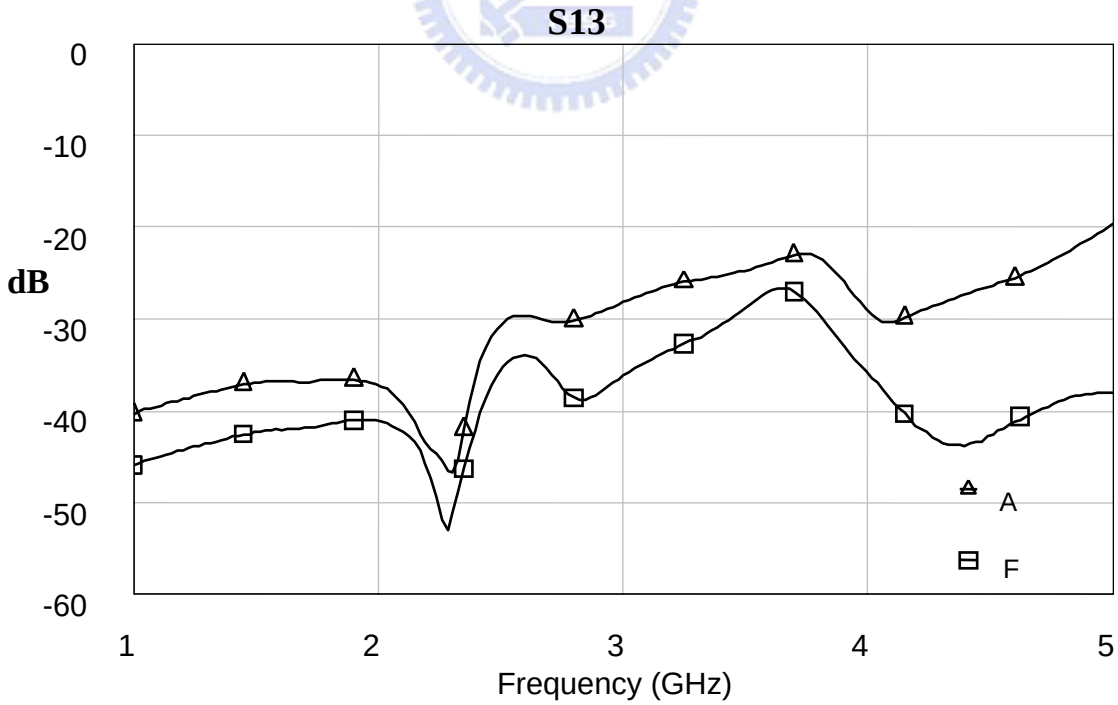

Fig 4-19 Measured isolation S13 in case A and F.

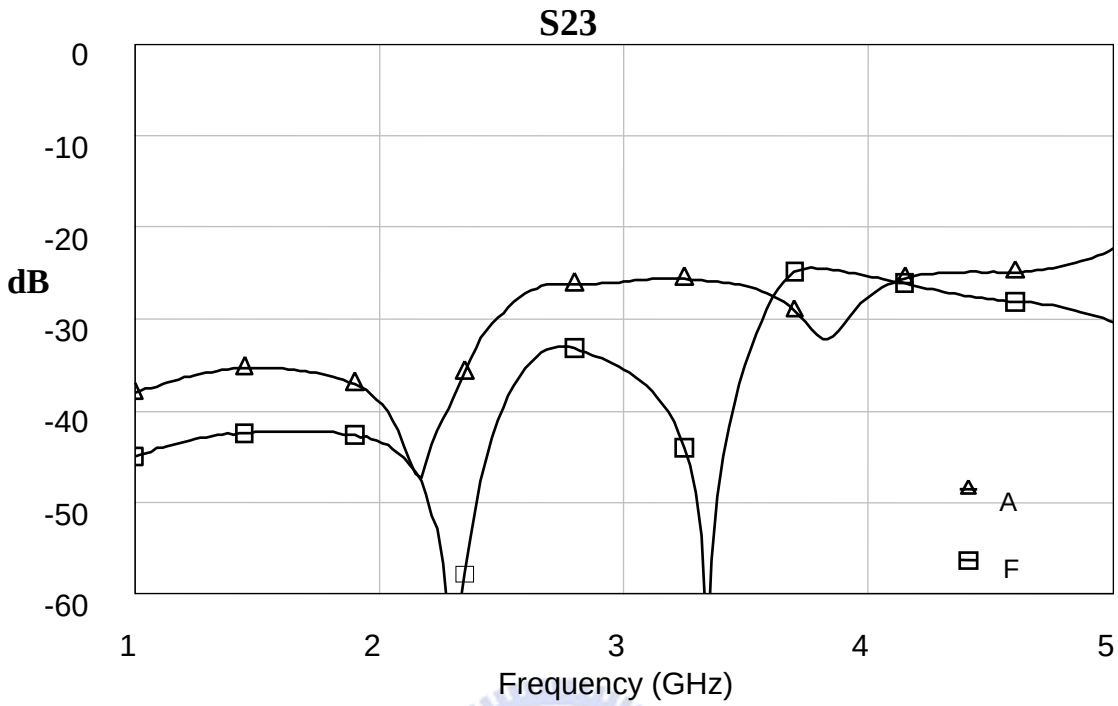

Fig 4-20 Measured isolation S23 in case A and F.

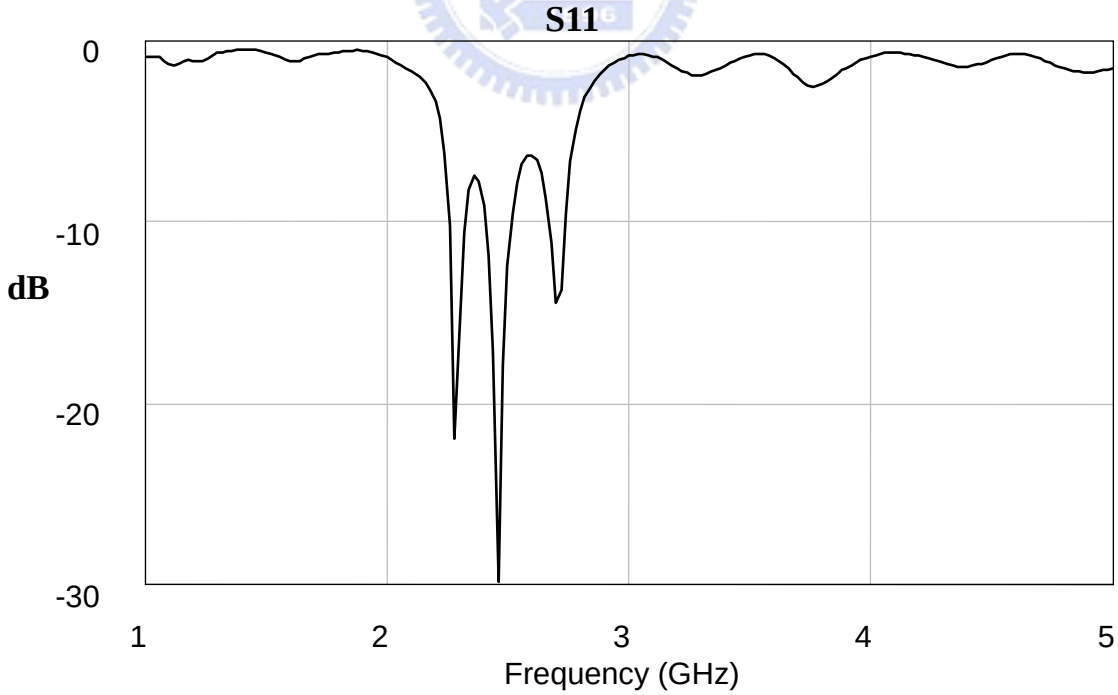

Fig 4-21 Measured return loss of BPF with on-package PIFA in case B.

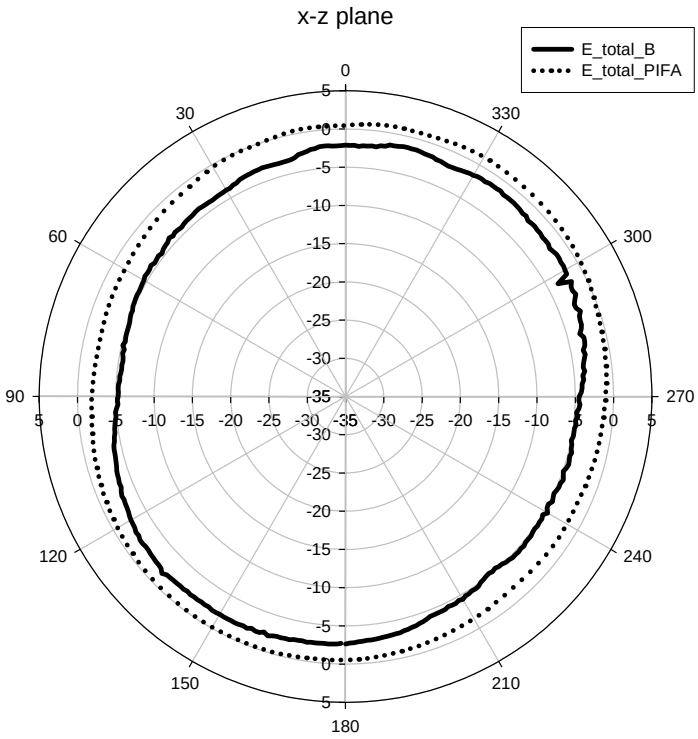

Fig 4-22a Measured radiation pattern of on-package PIFA with and without BPF at x-z plane (2.45GHz).

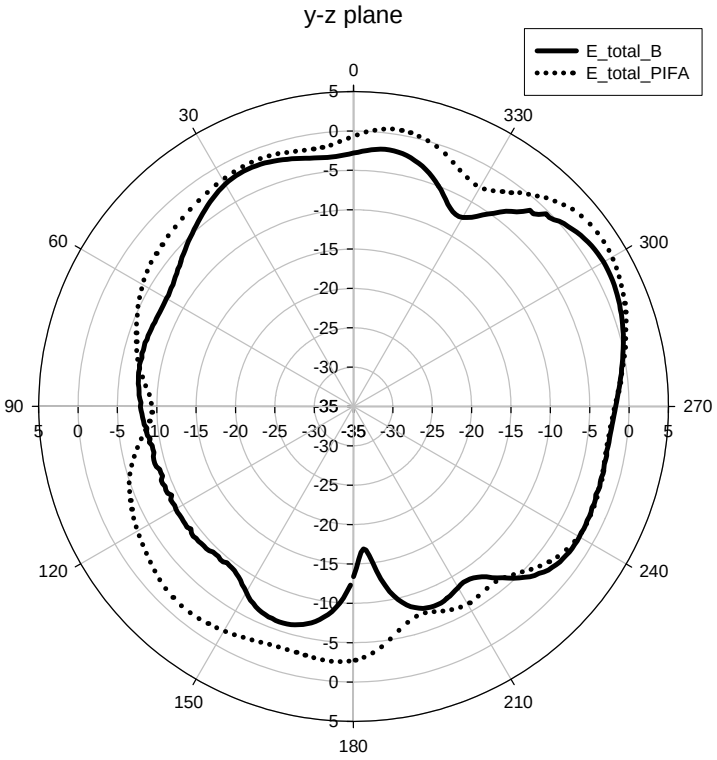

Fig 4-22b Measured radiation pattern of on-package PIFA with and without BPF. at y-z plane (2.45GHz).

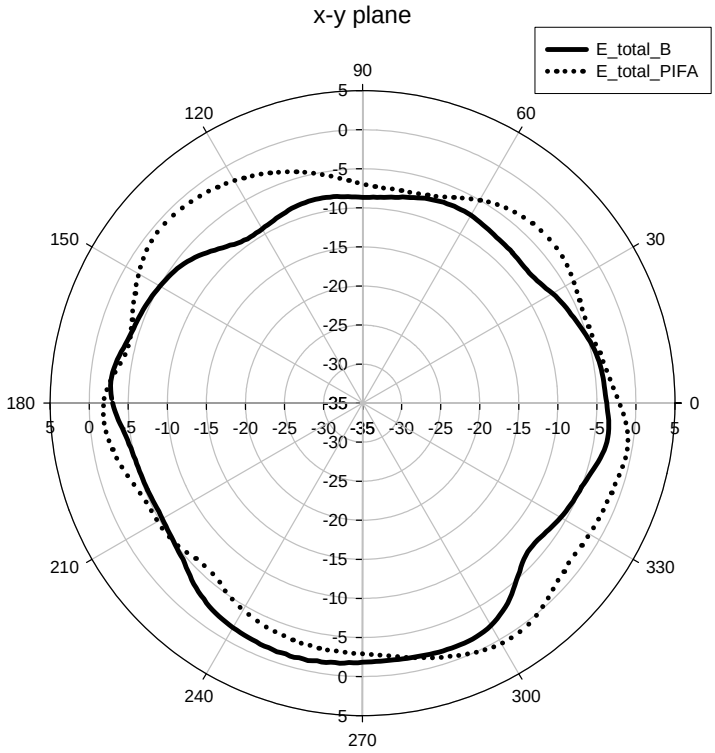

Fig 4-22c Measured radiation pattern of on-package PIFA with and without BPF at x-y plane (2.45GHz).

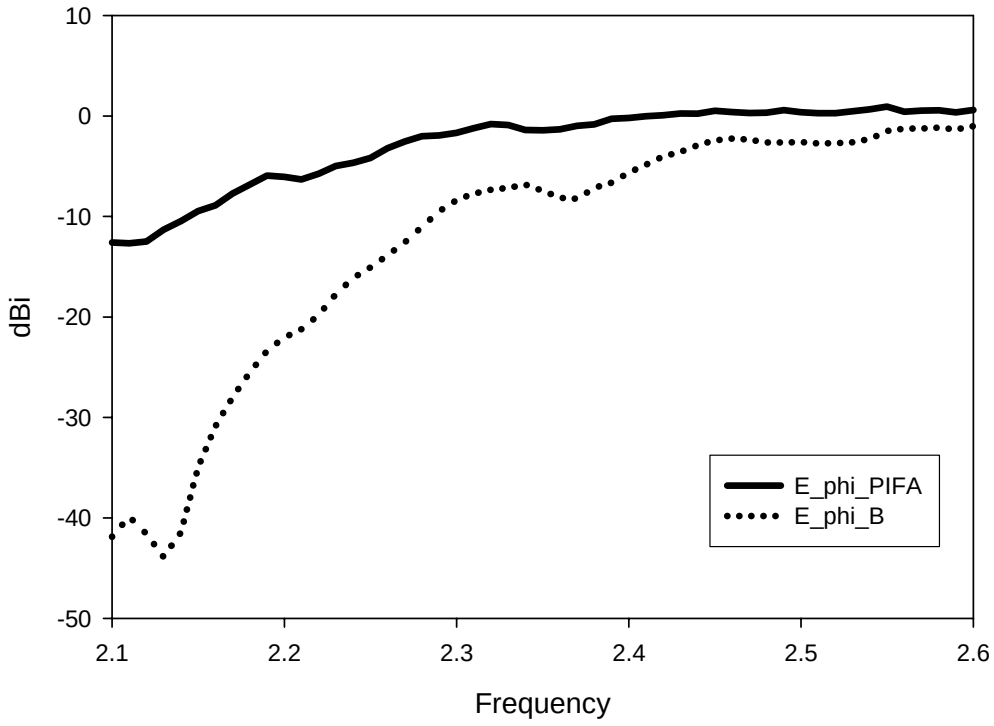

Fig 4-23 Gain vs. Frequency characteristic of the on-package PIFA with and without BPF at x-z plane.

Chapter 5

Conclusions

In this thesis, we presented an on-package planar inverted-F antenna for RF SOP application and also investigate the coupling effect between the on-package PIFA and the RF components in the shielding package.

In chapter 3, we introduce the design methodology of the on-package PIFA with and without ceramic materials. The ceramic materials can be excluded for cost reduction or other considerations. The influence of the different ground size and shielding package is also discussed. The performance of the on-package PIFA has merely changed when the ground size changes from 20×40 mm^2 to 20×45 mm^2. The planar element does not have not to be redesigned when the package changes from $15 \times 15 \times 1.5$ mm^2 to $15 \times 20 \times 1.5$ mm^3.The compact on-package PIFA has achieved the impedance bandwidth of 6.55% from 2.37 to 2.53GHz and an average gain of -0.63dBi at x-z plane. In chapter 4, it was observed that the performances of the antenna and RF passive components have merely change and the best isolation between the antenna and RF passive components can be achieved when the components have been appropriately arranged in the package.

The future work is to implement a WLAN RF module with the on-package PIFA. The WLAN RF module consists of an antenna, a T/R switch, a band-pass filter, a low-pass filter, and a power amplifier. Furthermore, a WLAN chip can also be realized with the transceiver chip and the on-package PIFA.

References

[1] Kyutae Lim; Obatoyinbo, A.; Davis, M.; Laskar, J.; Tummala, R., "*Development of planar antennas in multi-layer packages for RF system-on-a-package applications*", Electrical Performance of Electronic ackaging, 2001, page(s):101 – 104.

[2] Steyaert, M.; Borremans, M.; Janssens, J.; de Muer, B.; Itoh, I.; Craninckx, J.; Crols, J.; Morifuji, E.; Momose, S.; Sansen, W., "*A single-chip CMOS transceiver for DCS-1800 wireless communications*", Solid-State Circuits Conference, 1998, page(s):48 - 49, 411.

[3] Cambridge Silicon Radio: *CSR's single-chip bluetooth radio system*, U.K, 2001.

[4] Y. P. Zhang, "*Finite-difference time-domain analysis of integrated ceramic ball grid array package antenna for highly integrated wireless transceivers*", Antennas and Propagation, IEEE Transactions on, 2004, page(s):435 – 442.

[5] Warren L. Stuzman; Gary A. Thiele, "*Antenna theory and design*". 2nd edition, John Wiley & Sons, INC, 1998.

[6] Shyh-Jong Chung, "*Antenna design for wireless communication*", class notes.

[7] Kazuhiro Hirasawa and Misao Haneishi, "*Analysis, design, and measurement of small and low-profile antennas*", Artech House, INC, 1992.

[8] Y. P. Zhang, "*Integrated circuit co-fired laminated ceramic package antenna*", Solid-State and Integrated-Circuit Technology, 2001, page(s):100 - 103 vol.1.

[9] Y. P. Zhang, "*Integrated circuit ceramic ball grid array package antenna*", Antennas and Propagation, IEEE Transactions on, 2004, page(s):2538 – 2544.

[10] Y. P. Zhang, "*Integration of microstrip antenna on cavity-down ceramic ball grid array package*", Electronics Letters, Oct 2002, page(s):1307 – 1308.

[12] Y. P. Zhang, "*Design of on-package microstrip antennas for single-chip wireless transceivers*", Electronics Packaging Technology Conference, 2002, page(s):40 –

44.

[13] Tentzeris, M.M.; Laskar, J.; Papapolymerou, J.; Pinel, S.; Palazzari, V.; Li, R.; DeJean, G.; Papageorgiou, N.; Thompson, D.; Bairavasubramanian, R.; Sarkar, S.; Lee, J.-H., *"3-D-integrated RF and millimeter-wave functions and modules using liquid crystal polymer (LCP) system-on-package technology"*, Advanced Packaging, IEEE Transactions on, 2004, page(s):332 – 340.

[14] Chang-Ho Lee; Sutono, A.; Sangwoo Han; Kyutae Lim; Pinel, S.; Tentzeris, E.M.; Laskar, J., *"A compact LTCC-based Ku-band transmitter module"*, Advanced Packaging, IEEE Transactions on, 2002, page(s):374 – 384.

[15] Li-Rong Zheng; Xingzhong Duo; Meigen Shen; Torrika, T.; Michielsen, W.; Tenhunen, H.; Liu Chen; Gang Zou; Johan Liu, *"Design and implementation of system-on-package for radio and mixed-signal applications"*, High Density Microsystem Design and Packaging and Component Failure Analysis, 2004, page(s):97 – 104.

[16] Sudo, T.; Sasaki, H.; Masuda, N.; Drewniak, J.L., *"Electromagnetic interference (EMI) of system-on-package (SOP)"*, Advanced Packaging, IEEE Transactions on, 2004, page(s):304 – 314.

[17] Ching-Wen Tang; Yin-Ching Lin; Chi-Yang Chang, *"Realization of transmission zeros in combline filters using an auxiliary inductively coupled ground plane"*, Microwave Theory and Techniques, IEEE Transactions on, 2003, page(s):2112 – 2118.